



HAL
open science

Evaporation of Sessile Droplets of Polyelectrolyte/Surfactant Mixtures on Silicon Wafers

Andrew Akanno, Lionel Perrin, Eduardo Guzmán, Sara Llamas, Victor Starov, Francisco Ortega, Ramón Rubio, Manuel Velarde

► **To cite this version:**

Andrew Akanno, Lionel Perrin, Eduardo Guzmán, Sara Llamas, Victor Starov, et al.. Evaporation of Sessile Droplets of Polyelectrolyte/Surfactant Mixtures on Silicon Wafers. *Colloids and Interfaces*, 2021, 5 (1), pp.12. 10.3390/colloids5010012 . hal-03196232

HAL Id: hal-03196232

<https://hal.science/hal-03196232>



Submitted on 12 Apr 2021

HAL is a multi-disciplinary open access archive for the deposit and dissemination of scientific research documents, whether they are published or not. The documents may come from teaching and research institutions in France or abroad, or from public or private research centers.

L'archive ouverte pluridisciplinaire **HAL**, est destinée au dépôt et à la diffusion de documents scientifiques de niveau recherche, publiés ou non, émanant des établissements d'enseignement et de recherche français ou étrangers, des laboratoires publics ou privés.

Article

Evaporation of Sessile Droplets of Polyelectrolyte/Surfactant Mixtures on Silicon Wafers

Andrew Akanno¹, Lionel Perrin^{2,*}, Eduardo Guzmán^{1,3} , Sara Llamas¹, Victor M. Starov⁴, Francisco Ortega^{1,3}, Ramón G. Rubio^{1,3,*}  and Manuel G. Velarde³

¹ Departamento de Química Física, Facultad de Ciencias Químicas, Universidad Complutense, Ciudad Universitaria s/n, 28040 Madrid, Spain; drewakanno@gmail.com (A.A.); eduardogs@quim.ucm.es (E.G.); sarallamas@pdi.ucm.es (S.L.); fortega@quim.ucm.es (F.O.)

² Institut Lumière Matière, Claude Bernard University Lyon 1, Bâtiment Alfred Kastler-4ème Etage Domaine Scientifique de La Doua, 10 Rue Ada Byron, 69622 Villeurbanne CEDEX, France

³ Instituto Pluridisciplinar, Universidad Complutense, Paseo Juan XXIII 1, 28040 Madrid, Spain; mgvelarde@pluri.ucm.es

⁴ Chemical Engineering Department, Loughborough University, Epinal Way, Loughborough LE11 3TU, UK; v.m.starov@lboro.ac.uk

* Correspondence: l.perrin88@gmail.com (L.P.); rgrubio@quim.ucm.es (R.G.R.); Tel.: +34-394-4107 (R.G.R.)

Abstract: The wetting and evaporation behavior of droplets of aqueous solutions of mixtures of poly(diallyldimethylammonium chloride) solution, PDADMAC, with two different anionic surfactants, sodium laureth sulfate, SLES, and sodium *N*-lauroyl *N*-methyl taurate, SLMT, were studied in terms of the changes of the contact angle θ and contact length L of sessile droplets of the mixtures on silicon wafers at a temperature of 25 °C and different relative humidities in the range of 30–90%. The advancing contact angle θ_a was found to depend on the surfactant concentration, independent of the relative humidity, with the mixtures containing SLES presenting improved wetting behaviors. Furthermore, a constant droplet contact angle was not observed during evaporation due to pinning of the droplet at the coffee-ring that was formed. The kinetics for the first evaporation stage of the mixture were independent of the relative humidity, with the evaporation behavior being well described in terms of the universal law for evaporation.

Keywords: spreading; evaporation; polyelectrolyte; surfactant; sessile droplet; contact angle.



Citation: Akanno, A.; Perrin, L.; Guzmán, E.; Llamas, S.; Starov, V.M.; Ortega, F.; Rubio, R.G.; Velarde, M.G. Evaporation of Sessile Droplets of Polyelectrolyte/Surfactant Mixtures on Silicon Wafers. *Colloids Interfaces* **2021**, *5*, 12. <https://doi.org/10.3390/colloids5010012>

Academic Editor:
Alexander Kamyshny

Received: 14 January 2021
Accepted: 14 February 2021
Published: 16 February 2021

Publisher's Note: MDPI stays neutral with regard to jurisdictional claims in published maps and institutional affiliations.



Copyright: © 2021 by the authors. Licensee MDPI, Basel, Switzerland. This article is an open access article distributed under the terms and conditions of the Creative Commons Attribution (CC BY) license (<https://creativecommons.org/licenses/by/4.0/>).

1. Introduction

The evaporation of fluids is of paramount interest for many technological applications, including spray evaporation [1], hydrological cycles [2], oil–water separation [3], liquid hydrocarbon evaporation and combustion [4,5], phase change heat transfer [6] and power generation [7]. Many coupled factors dominate the evaporation process: heat and mass flows, thermocapillarity, substrate thermal conductivity and deformability, substrate patterning, surface curvature, and the formation of deposits. The decoupling of these processes is currently extremely difficult with current experimental and theoretical methods [8–12]. The situation is even more difficult when complex fluids—such as those frequently found in technological applications—are concerned because the prediction and control of the evaporation of fluid droplets becomes essential for the appropriate design of the abovementioned processes.

Despite the fact that in most practical applications pure fluids are replaced by mixtures or suspensions, little work has been done in terms of providing predictions and detailed analyses of such systems. Furthermore, the behavior of such systems depends on the nature of the components, the structures formed in the bulk and their adsorption kinetics at both the liquid/vapor and solid/liquid interfaces [13–17]. It is worth mentioning that the application of theories accounting for the behavior of pure fluids provides a semiquantitative prediction of the first stage of evaporation when nanoemulsions [18] and

surfactant solutions [19] are concerned. The removal of the excess solvent from droplets of colloidal suspensions can lead to deposits of solutes onto substrates whose surfaces are usually rough. During evaporation, the droplet contact line can become pinned at a defect on the substrate surface for a significant period of time due to the balance between capillary-pressure and disjoining-pressure gradients. The pinning of the contact-line limits the motion of the contact line on solid surfaces and accelerates droplet solidification, leading to particle deposition near the droplet edge, forming a coffee-ring pattern, with pinning being a key factor in determining solute deposition patterns and the evaporation rate [20–23]. The above discussed phenomena may appear on the surface of hair fibers during the drying of water after shampooing [24]. During such a process, it is possible to consider up to three different processes governing the spreading and evaporation of water droplets: (i) adsorption of surface active materials to the liquid/vapor interface; (ii) deposition on the hair fiber surface, and (iii) water evaporation. However, a direct evaluation of the process is difficult due to the complexity of hair as substrate (chemical and topological heterogeneity) and the multicomponent character of shampoo formulations.

Aqueous solutions containing mixtures of polyelectrolytes and surfactants bearing opposite charges are generally considered as simplified models for conditioner formulations. Hence, the study of the behavior of these systems in solutions and upon their adsorption at interfaces—both fluid/fluid and fluid/solid—may help in understanding the main physico-chemical bases governing the processes involving the performance of shampoos [25,26]. In particular, the performance of hair conditioner formulations is related to the layer of polyelectrolyte–surfactant complexes adsorbed on the hair fibers after drying the hair [27–32]. It should be noted that together with the cosmetic industry, polyelectrolyte–surfactant mixtures are widespread in many other industries, ranging from detergency to tertiary oil recovery, and from dietary products and pharmaceuticals to wood pulping [27,33–35], with the understanding of the combined effect of evaporation and adsorption of surface active compounds to the involved interfaces being critical for their optimization [36,37].

This work describes the evaporation process of droplets of polyelectrolyte–surfactant mixtures deposited onto silicon dioxide surfaces. Although the solid substrates used in this work are far from the complexity of real surfaces used in technological applications, and the pinning effect will for sure be stronger than in our substrates. The present model substrate will allow one to discuss various effects of the pinning on the evaporation process, and on the validity of the theory for describing the results before pinning. The optimization of the formulations makes it necessary to know the morphology of the deposit in order to minimize its friction coefficient. Moreover, the formulation of creams for skin cosmetics must also take into consideration the characteristics of the deposits after evaporation when the kinetics of cream penetration is slow compared with evaporation kinetics. This work discusses the behavior of aqueous solutions of mixtures formed by poly(diallyldimethylammonium chloride), PDADMAC, as polycation and two different anionic surfactants, sodium laureth sulfate (SLES) and sodium *N*-lauroyl-*N*-methyltaurate (SLMT). These mixtures have been chosen due to their widespread presence in commercially available cosmetic formulations.

2. The Stages of the Evaporation Process of a Sessile Droplet

A droplet of a liquid, which completely or partially wets a solid, spreads over the surface up to reach a maximum contact length, with the assumption that the liquid volume remains constant and that the evaporation is negligible during the fast spreading. Afterwards, evaporation of the liquid occurs, with the spreading being negligible [38].

The evaporation of droplets of partial wetting liquids may be generally described in terms of three different stages, as shown in Figure 1. During the first stage, the contact radius of the droplet remains constant, whereas the contact angle decreases down to the value corresponding to the receding contact angle θ_r , thus indicating contact angle hysteresis [39,40]. In the second stage the contact angle θ_r remains constant and the contact

length decreases. Finally, both the contact angle and the contact length decrease during a third stage until the drop vanishes [38].

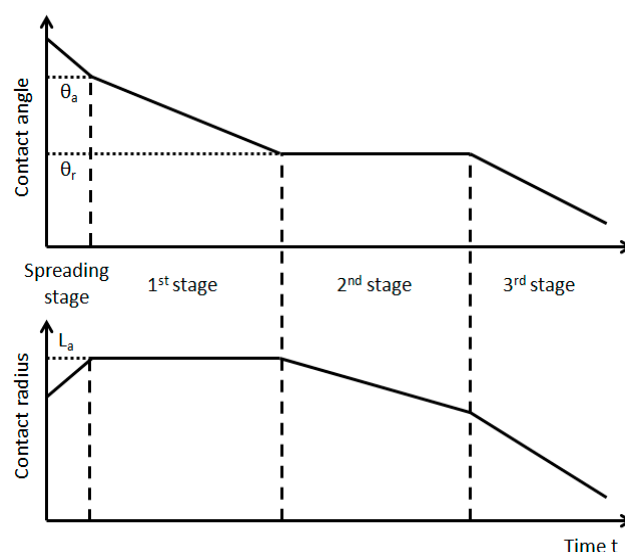


Figure 1. Scheme of the time evolution of the contact angle and the droplet radius during the different stages of the evaporation.

The theory has provided analytical expressions for the droplet volume, contact radius and contact angle dependencies on time for the first and second stages, accounting for the behavior of droplets of pure fluids: water and organic solvents on various substrates [41]. Although there is an appropriate theoretical description of the behavior of pure liquid droplets during the first two stages of evaporation, the driving force and kinetics of the third stage are not yet well understood. It is reasonable to assume that the kinetics of the third stage are strongly influenced by the Derjaguin pressure acting in the region of the three-phase contact line. On the other hand, for surfactant solutions, it has recently been shown that the theoretical predictions do not agree with the experimental results for the second stage. Similar conclusions were found for nanoparticle suspensions, although in this case there is a strong pinning–depinning process of the three-phase contact line that is not taken into account by the above theories [19,42,43].

The main details of the theory that describes the first and second evaporation stages of pure fluids—that is also suitable for describing the first evaporation stage of more complex systems, such as surfactant mixtures or nanosuspensions—are summarized in the Appendices A–C [18,19].

3. Materials and Methods

3.1. Chemicals

PDADMAC with an average molecular weight in the 100–200 kDa range was purchased as a 20 wt% aqueous solution from Sigma-Aldrich (San Louis, MO, USA) and was used as received. The anionic surfactant SLES, with an average number of 2 oxyethylene, was supplied by Kao Chemical Europe S.L. (Barcelona, Spain) as an aqueous solution of 70 wt% of surfactant concentration. It was purified by lyophilization followed for recrystallization of the obtained powder using acetone for HPLC (Acros Organics N.V., Geel, Belgium) [44]. SLMT was synthesized and purified following the procedure described in our previous publication [45].

Ultrapure deionized water used for cleaning and solution preparation was obtained by a multicartridge purification system aquaMAX™-Ultra 370 Series (Young Lin Instrument, Co., Gyeonggi-do, South Korea). The water used had a resistivity higher than 18 MΩ·cm, and a total organic content lower than 6 ppm.

3.2. Polyelectrolyte–Surfactant Aqueous Mixtures Preparation

Aqueous solutions of polyelectrolyte–surfactant mixtures, containing a fixed PDADMAC concentration of 5 g/L and different surfactant concentrations in the range of 10^{-6} - 5 mM were used. It is worth mentioning that polyelectrolyte–surfactant solutions frequently lead to kinetically arrested non-equilibrium structures [44,46–48]. For this reason, it is paramount to always adopt the same protocol for the preparation of solutions.

The preparation of the aqueous mixtures used in this work was performed following a procedure that was adapted from our previous studies [29,30,45,49,50]. This procedure can be briefly summarized in the following steps: (i) the required amount of an aqueous commercial solution of PDADMAC (concentration 200 g/L) for obtaining final mixtures with a polymer concentration of 5 g/L was weighted and poured into a flask; (ii) surfactant was added and this was diluted accordingly to reach final concentration. For this purpose, surfactant solutions (pH \sim 5.6) with concentrations one order of magnitude higher than the final surfactant concentration in the mixture were weighted and added to the flask containing PDADMAC; (iii) the mixture was diluted with an acetic acid solution of pH \sim 5.6 to the final bulk composition. During the mixture preparation, there was no delay between the addition of different components. The final mixtures were homogenized by mild stirring at 1000 rpm using a magnetic stirrer for one hour at room temperature and then they were left to age for 1 week prior to use. This aging period was used to ensure that no turbidity appears in the mixtures and that the transparency of the mixtures after preparation was maintained [45]. The above procedure has been shown to demonstrate a good level of reproducibility for obtaining kinetically arrested states after mixing polymers and surfactants [45,50].

The pH of all the solutions was fixed at 5.6 using glacial acetic acid (purity > 99 %). It should be noted that the pH, the PDADMAC concentration, and the use of acetic acid for fixing the pH were not an arbitrary choice. Such conditions were adopted to mimic the characteristics of hair-conditioning formulations used for reducing the bleaching of hair fibers under application conditions [34,51,52].

3.3. Techniques

The experiments performed in this study were focused on three different aspects of polyelectrolyte–surfactant mixtures: (i) polyelectrolyte–surfactant association in solution; (ii) adsorption of polyelectrolyte–surfactant aqueous mixtures to interfaces (both solid/liquid and liquid/vapor), and (iii) evaporation and spreading of droplets of polyelectrolyte–surfactant aqueous mixtures on silicon wafers. All experiments were carried out at 25.0 ± 0.1 °C.

3.3.1. Polyelectrolyte–Surfactant Association in Solution

The association of the polyelectrolyte and the surfactant was evaluated in terms of the turbidity of the aqueous mixtures and the binding degree of the surfactant to the polyelectrolyte chains.

The turbidity of the solutions was evaluated from their transmittance at 400 nm, obtained using a UV-Visible spectrophotometer (HP-UV 8452, Hewlett Packard, Palo Alto, CA, USA). The turbidity of the samples was determined at 400 nm (turbidity = $(100 - T[\%])/100$, where T is the transmittance). It is worth mentioning that neither the polyelectrolyte nor the surfactant present any absorption band above 350 nm.

The binding isotherm of the surfactant to the polyelectrolyte chains was determined by potentiometric titration using a surfactant selective electrode model 6.0507.120 from Metrohm AG (Herisau, Switzerland). The binding degree of surfactant β is estimated from the potentiometric measurements as [53]

$$\beta = \frac{c_s^{bound}}{c_{monomer}} \quad (1)$$

with c_s^{bound} and $c_{monomer}$ being the concentrations of surfactant bound to the polymer chains and charged monomers on the polyelectrolyte chains, respectively. The determination of the binding isotherm using surfactant selective electrodes firstly requires one to obtain a calibration curve using surfactant solutions in the same concentration range used for the preparation of the polyelectrolyte–surfactant mixtures. For this purpose, the electromotive forces (EMF) of surfactant solutions are first recorded using the surfactant selective electrode connected to a pH-meter (model CG842-Schott Instruments GmbH, Mainz, Germany). This permits the construction of a calibration curve by plotting the recorded EMF against the surfactant concentration. The comparison of the calibration curve with the EMF dependence on the surfactant concentration obtained for polyelectrolyte–surfactant mixtures, following the above described procedure, provides an evaluation of the number of free surfactant molecules remaining in the solution when the mixture is considered. Thus, this allows one to determine the amount of surfactant that remains free in the solution when the mixture is determined from the surfactant concentration on the calibration curve, which presents the same EMF as that obtained for the mixture.

3.3.2. Adsorption of Polyelectrolyte–Surfactant Aqueous Mixtures to Interfaces

The absorption of polyelectrolyte–surfactant complexes formed in solution with the liquid/vapor and solid/liquid interfaces was analyzed by surface tension and quartz crystal microbalance with dissipation monitoring (QCM-D) measurements, respectively.

The adsorption of surfactant and polyelectrolyte–surfactant aqueous solutions was followed by the surface tension dependences on the surfactant concentration measured using a home-made profile analysis tensiometer in pendant drop configuration (for further details see reference [45,49,54]). This tensiometer also allows one to obtain an evaluation of the time evolution of the surface tension, giving access to the adsorption kinetics at the liquid/vapor interface. The adsorption at the liquid/vapor interface was measured until steady state was reached, i.e., changes of surface tension smaller than $0.1 \text{ mN}\cdot\text{m}^{-1}$ during 30 min. Special care was taken to minimize the evaporation effects during these experiments.

The adsorption of the polyelectrolyte–surfactant aqueous solution to the solid/liquid interface was measured using a QCM-D (QCM Z500 from KSV, Espoo, Finland) fitted with a silicon dioxide-coated AT-cut quartz crystals. These crystals were cleaned with piranha solution (70% sulfuric acid/30% hydrogen peroxide) for 30 min, and then thoroughly rinsed with pure water and ethanol. Afterwards, the substrates were dried with a nitrogen stream and stored in a desiccator until use. QCM-D measures the impedance spectra of a quartz crystal for the fundamental frequency ($f = 5 \text{ MHz}$) and for the odd overtones up to the 11th. The impedance spectra were analyzed using a single layer model following the procedure described by Voinova et al. [55,56]. This method allows one to relate the changes in the resonant frequency Δf and dissipation factor ΔD of the different overtones (note that fundamental frequency is not considered for data analysis due to its high noise to signal of its signal) to the surface excess at the solid/liquid interface Γ_{sl} .

3.3.3. Evaporation and Spreading of Droplets of Polyelectrolyte–Surfactant Aqueous Mixtures on Silicon Wafers

The evaporation and spreading of droplets of polyelectrolyte–surfactant aqueous mixtures on silicon wafers was followed by measurements of the contact angles of the droplets using a home-made goniometer adapted from that described in reference [57]. This experimental setup consisted of a cylindrical steel chamber (13 cm of diameter, 10 cm of depth) fitted with flat borosilicate plate windows on the sides, a lead glass window on the top cover and toughened glass at the bottom of the chamber. The side windows and the glass bottom were positioned in such a way that allows one to follow the time evolution of the droplet shape. Top and side view images of the drop shape were captured using a CCD camera (KODAK IT CCD KAI340). The camera captures images of the frame size 640×480 pixels at a maximum rate of 60 frames per second. Flat windows were used in the measuring chamber to avoid any optical aberration effects.

Droplets of the samples (2–4 μL) were manually dispensed using a Hamilton microliter syringe (SN 701, 10 μL). This droplet size is suitable for ensuring that the spherical cap shape is maintained [18] and to avoid any significant buoyancy convection effects [58,59]. The droplets were carefully placed on the surface of the substrate (Silicon wafers, 2.54 cm of diameter, from Siltronix, France) by bringing the droplet formed at the tip of the syringe in direct contact with the substrate surface. The silicon wafers were cleaned following the same procedure used for the sensors used in QCM-D experiments. This procedure results in the formation of a homogeneous layer of hydrophilic silicon on the wafer surface, with a thickness in the range of 2–3 nm, as was determined by ellipsometry. Meanwhile the water contact angle and zeta potential were similar to that of a damaged hair fiber surface [27]. Special care was taken to ensure that the concentrations of the solutions were identical by measuring several drops from the same stock and at least two different stocks; this is important to ensure that the chemical potential of the different species was the same [60]. The results obtained for the contact angle measurements coincided with the experimental uncertainty.

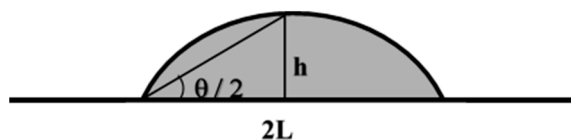
Experiments were performed at three different relative humidity values: 30, 60 and 90%. Saturated aqueous solutions of potassium chloride and potassium sulfate were employed to control the relative humidity of the measuring chamber at 60 and 90%, respectively. The temperature of the measuring chamber was kept at 25.0 ± 0.2 °C.

The side view image of the sessile droplets was analyzed by the axisymmetric drop shape analysis profile (ADSA-P) method [61] to obtain the contact length $2L$ and height h of the sessile droplet (see Scheme 1). The contact angle θ and volume V of the sessile droplet was estimated assuming that the drop has a spherical-cap shape and therefore (see Equations (2) and (3)),

$$\frac{\theta}{2} = \tan^{-1} \left(\frac{h}{L} \right), \quad (2)$$

and

$$V = \frac{\left[\frac{\pi}{3} (L)^3 \right] (1 - \cos \theta)^2 (2 + \cos \theta)}{\sin^3 \theta}, \quad (3)$$



Scheme 1. Definition of the variables used in Equations (2) and (3) for a spherical-cap droplet.

4. Results and Discussion

4.1. PDADMAC–Surfactant Association in Solution

The analysis of any phenomena involving polyelectrolyte–surfactant mixtures requires a careful examination of the interactions occurring in solution between the polyelectrolyte chains and the oppositely charged surfactant mixtures. These interactions, commonly driven by a combination of electrostatic and hydrophobic interactions, lead to the formation of polyelectrolyte–surfactant complexes, which can present a broad range of physico-chemical properties and structures depending on several factors, e.g., the nature of the polyelectrolyte and surfactant, the polyelectrolyte/surfactant ratio or mixing protocol [62,63]. For the particular case of the PDADMAC–SLMT and PDADMAC–SLES mixtures, the association and characteristics of the polymer–surfactant aggregates, obtained following the same mixing protocol as that used in this study, were discussed in our previous publications [28,29,45,49,50] and in this section a summary of the main findings will be presented.

A very important aspect to consider before analyzing the association of PDADMAC with SLMT and SLES is the high polymer concentration (5 g/L) used in this study. This means that even for the highest surfactant concentration there is an excess of monomers

in relation to the number of surfactant molecules, and hence all the studied compositions belong to a one-phase equilibrium region of the phase diagram, containing undercompensated positively charged polyelectrolyte–surfactant complexes. This is easily understood considering that even for surfactant concentrations of about 1 mM, the number of monomers available is 30-fold higher than the number of added surfactant molecules [45,49]. This agrees so far with the results shown for the binding isotherm (see inset of Figure 2), which allows one to assume the total binding of the surfactant molecules to the polyelectrolyte chains, and consequently, the formation of undercompensated monomers with an excess of positive charges. Therefore, the formation of transparent aqueous solutions of polyelectrolyte–surfactant complexes within the entire explored surfactant concentration range should be expected. However, this is not the case for PDADMAC–SLMT mixture nor for PDADMAC–SLES mixtures, as evidenced by the concentration dependences of the turbidity of the mixtures displayed in Figure 2 [28,29].

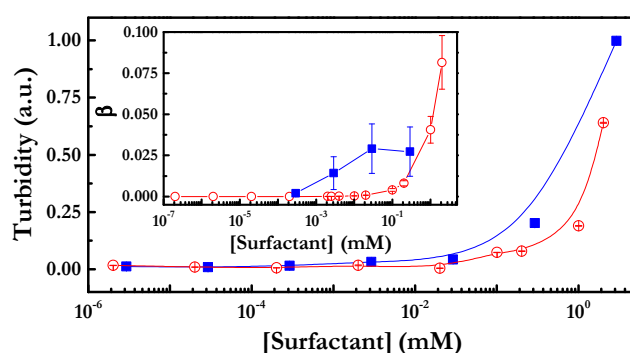


Figure 2. Surfactant concentration dependences of the turbidity of the poly(diallyldimethylammonium chloride) solution (PDADMAC)–surfactant aqueous solutions as was measured at 400 nm. The inset shows the binding isotherms for PDADMAC–surfactant aqueous solutions as were obtained by potentiometric titration. In both panels: PDADMAC–sodium *N*-lauroyl *N*-methyl taurate (SLMT) (■) and PDADMAC–sodium laureth sulfate (SLES) (○). Lines are intended to act as a guide.

The increase in the turbidity of the mixtures for the highest surfactant concentrations can be only explained by the formation of solid particles due to the polyelectrolyte–surfactant association. This is only possible assuming that the formation of kinetically-trapped aggregates occurs due to the Marangoni stresses associated with a local excess of surfactant molecules during the initial stages of the mixing procedure [64–68]. These kinetically-trapped aggregates remain intact upon dilution and present a quasi-neutral inner core formed mainly of surfactant molecules bound to the polymer monomers, where the external region appears positively charged, i.e., formed by non-associated monomers. This picture is compatible with the positive charge of the complexes, as was reported in our previous work [28,29], which provides the complexes with colloidal stability, i.e., precipitation of the kinetically-trapped complex is not observed. Therefore, the presence of kinetically-trapped polyelectrolyte–surfactant particles pushes the system to the onset of a two phase region for compositions far from the real equilibrium two phase region.

4.2. Adsorption at the Liquid/Vapor Interface

The adsorption of polyelectrolyte–surfactant mixtures at the liquid/vapor interface is a dynamic process which can be studied following the temporal evolution of the surface tension during the adsorption process, i.e., the dynamic surface tension. Figure 3 shows the adsorption kinetics as the time dependence of the surface tension for both mixtures, obtained using the drop shape tensiometer.

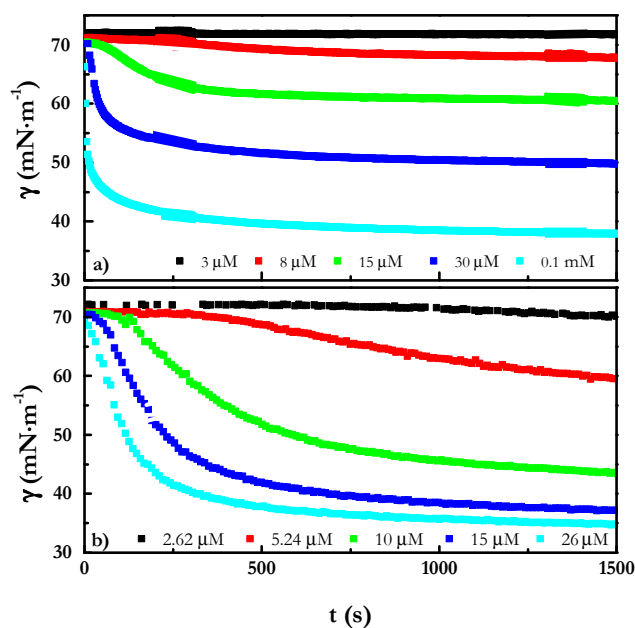


Figure 3. Dynamic surface tension isotherms as were obtained using a drop shape tensiometer for the adsorption of PDADMAC–surfactant mixtures, with different surfactant concentrations, at the liquid/vapor interface. (a) PDADMAC–SLMT and (b) PDADMAC–SLES.

The results show differences in the time dependences of the surface tension of the liquid/vapor for mixtures of PDADMAC with SLMT and SLES. The adsorption of PDADMAC–SLMT mixtures occurs with a monotonous decrease in the surface tension with time from the initial stages of the adsorption process. This suggests that the adsorption of the surface active species probably occurs without any further reorganization at the interface upon their trapping at the liquid/vapor interface. On the other side, a two-step adsorption is observed for the adsorption of PDADMAC–SLES mixtures at the liquid/vapor interface. At short times, a concentration dependent induction period is found that may be related to an initial accumulation of surface active species at the interface. Once the surface coverage overcomes a threshold value, the reorganization of the adsorbed materials occurs at the interface, enabling further adsorption of surface active species. This leads to a decrease in the surface tension with time, eventually reaching the layer equilibration. The above commented differences on the equilibration mechanisms of the liquid/vapor interfaces upon the adsorption of mixtures of PDADMAC with SLMT and SLES may be rationalized in terms of the chemical nature of the surfactants and their interaction with the interface. Thus, the hydrophobic tail of SLMT, an alkyl tail, tries to minimize its contact points with water, and hence, PDADMAC–SLMT complexes tend to remain in a compact conformation even upon their incorporation to the liquid/vapor interface. This results in a monotonous decrease in the surface tension from the initial states of the adsorption. On the other side, SLES contains oxyethylene groups within its hydrophobic tail, and this favors the formation of hydrogen bonds with water. This leads to a situation in which, after the initial trapping of the complexes at the liquid/vapor interface occurring during the induction period, the PDADMAC–SLES can dissociate and spread at the interface leading to a strong decrease in the surface tension that appears after the induction period. The distribution of the PDADMAC–SLES complexes at the liquid/vapor interface is favored by the hydrogen bonding of the SLES molecules and water, which appears to be hindered in the solution. Further details on the mechanical basis of the layer equilibration process can be found in previous work [49,50,69–71]. It is true that the above picture seems to be counterintuitive. However, it is assumed that the equilibrium implies that the chemical potential, μ , of each species is the same in bulk, liquid/vapor and/or solid/liquid interfaces, with the values of μ depending on the interactions between components—including the hydrogen bonds—with the water. Such interactions may differ in the bulk and at the

interface. This may be especially critical in our system where kinetically trapped states are involved [68,69]. Therefore, it could be assumed that the existence of two main factors governing the adsorption—on one side the different hydrophobicity of the two surfactants, and on the other side, their different chemical structure—leads to different interactions with the polyelectrolyte. These two factors modify the structure, size and hydrophobicity of the polyelectrolyte–surfactant complexes, thus leading to different adsorption levels at interfaces.

It should be noted that this two-step adsorption mechanism expands over a time-scale longer than the adsorption of PDADMAC–SLMT mixtures. As mentioned above, polyelectrolyte–surfactant mixtures present a very important role in the performance of hair-conditioning formulations, and hence, a comparison of the time scale involved in their adsorption at interfaces, in relation to the typical use of capillary cosmetic products under the shower, may be interesting from a technological perspective. It is generally assumed that the application time for hair conditioners is about 120 s, which appears comparable to the time required for the equilibration of PDADMAC–surfactant layers at the liquid/vapor interface when the surfactant concentration is high, with the equilibration time being significantly increased, by up to one order of magnitude, for the lowest surfactant concentrations. It is true that the situation during the conditioning process is far from that which occurs at the liquid/vapor interface due to the shearing occurring during the application of the product. This may accelerate the adsorption to the liquid/vapor interface [51]. It should be noted that the adsorption kinetics of PDADMAC–surfactant mixtures to the liquid/vapor interface suggests a depletion of surface active species from the solution which may establish competition with the spreading and evaporation processes.

Understanding the equilibrium adsorption of PDADMAC–SLMT and PDADMAC–SLES mixtures at the liquid/vapor interfaces requires prior knowledge of the behavior of the PDADMAC, SLMT and SLES solutions at such an interface. Figure 4a shows the surface tension isotherms obtained after equilibration using a drop shape technique for solutions of the two surfactant and PDADMAC (see inset Figure 4a).

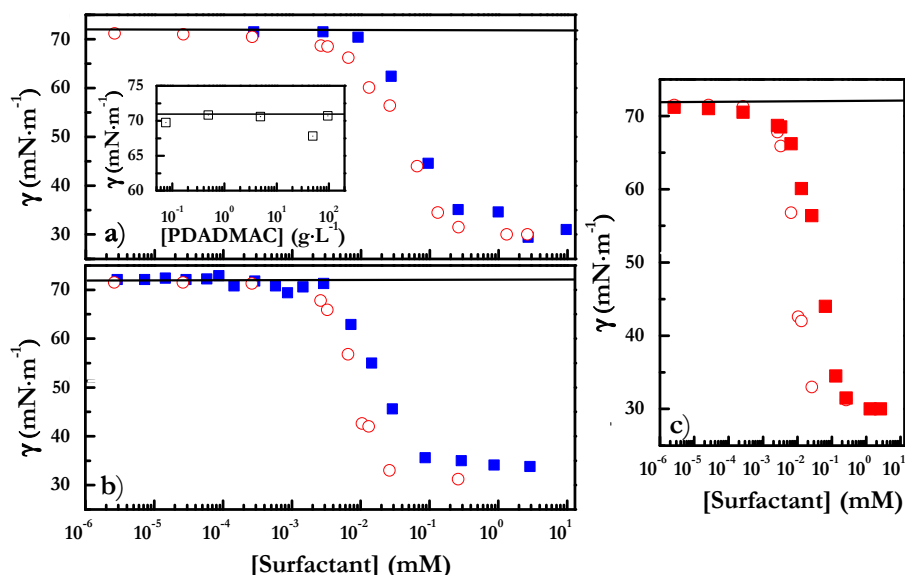


Figure 4. Surface tension isotherms, as were obtained using a drop shape tensiometer. (a) Surfactant solutions: SLMT (■) and SLES (○). The inset shows the surface tension isotherm for PDADMAC solutions as function of the concentration. (b) PDADMAC–surfactant solutions with a fixed polymer concentration of 5 g/L: PDADMAC–SLMT and (■) and PDADMAC–SLES (○). The solid lines represent the surface tension of the pure Milli-Q water used in this work. (c) Comparison of surfactant and PDADMAC–surfactant solutions: SLES (■) and PDADMAC–SLES with a fixed polymer concentration of 5 g/L (○). The solid lines represent the surface tension of the pure Milli-Q water used in this work.

PDADMAC solutions have a negligible effect on the surface tension of water (see inset in Figure 4a), in agreement with the absence of interfacial activity of PDAMAC reported by Noskov et al. [72] for solutions with concentrations below 30 g/L. On the contrary, the surface tension, γ , of both surfactants decreases with the increase in the bulk concentration up to the critical micelle concentration (CMC) of the surfactants, where a γ plateau was found. The values of CMC for SLMT and SLES were found to be 0.90 and 0.26 mM, respectively. It should be noted that the lower CMC value of SLES in relation to that of SLMT may appear counterintuitive due to the higher hydrophilicity of SLES (contains oxyethylene groups on its hydrophobic chains). However, the presence of oxyethylene groups on the SLES molecules results in the formation of ion–dipole interactions between such groups and the sulfonate polar head of SLES molecules. In particular, the existence of ion–dipole interactions between the oxyethylene groups, directly linked to the polar head on the SLES molecules and the sulfonate polar heads of nearby SLES molecules, results in micellization being favored, and hence, the CMC of SLES appears at surfactant concentrations lower than that expected for a surfactant containing alkyl chains as a hydrophobic domain [73,74]. Figure 4b shows the adsorption isotherms obtained for PDADMAC–SLMT and PDADMAC–SLES mixtures with a fixed PDADMAC concentration of 5 g/L. For the lowest surfactant concentrations, the adsorption behavior is similar for both mixtures due to the low surface coverage at the liquid/vapor interface, which is not enough to reduce the surface free energy. This low surface coverage region is followed by a monotonical decrease in the surface tension, at the intermediate bulk SLMT or SLES concentrations, up to reaching a γ -plateau for the highest concentrations of the surfactant. This plateau is associated with the maximum coverage of the interface, as was evidenced using neutron reflectometry, with the composition of the interfacial layer mirroring the bulk composition [45]. It is worth noting that the decrease in γ starts at surfactant bulk concentrations one order of magnitude lower for polyelectrolyte–surfactant mixtures than for pure surfactant solutions. This indicates that the interaction of PDADMAC and the surfactants at the liquid/vapor interface leads to a synergistic lowering of γ with respect to the pure components. This synergistic lowering of γ may be easily understood if consideration is given towards the absence of surface activity of the PDADMAC and the lower surface tension of PDADMAC–surfactant solutions in relation to that of the pure surfactant with the same concentration. The latter is evidenced from Figure 4c, where the comparison of the surface isotherms for SLES and PDADMAC–SLES solutions are displayed together. It should be noted that the synergistic lowering of the liquid/vapor surface tension on polyelectrolyte–surfactant mixtures is a well-accepted phenomenon [75], which results from the co-adsorption of the non-surface active polyelectrolyte combined with the oppositely charged polyelectrolyte [76].

The comparison of the surface tension vs. surfactant concentration for polyelectrolyte–surfactant mixtures points out some differences. The presence of the oxyethylene group in SLES makes it more hydrophilic than SLMT, which makes SLES more prone to form hydrogen bonds with water at the interface. This contributes to the dissociation and spreading of the complexes adsorbed at the interface unlike in the case of the more hydrophobic SLMT.

4.3. Spreading Behavior

We studied the surfactant concentration dependences of the wetting and evaporation behavior of PDADMAC–SLES and PDADMAC–SLMT, measuring the contact angle, θ , and contact radius, L , of the smooth silicon wafer surfaces of sessile droplets. It should be noted that the contact line remains circular during the whole spreading stage, as evidenced by the analysis of the images obtained using a camera, enabling viewing the droplets from above. The results are shown in Figure 4a,b and point out that the relative humidity has a negligible influence on the wetting behavior of the mixtures on the solid substrate.

Preliminary measurements for pure water droplets on the silicon wafer substrate result in a value of the advancing contact angle θ_a around $55 \pm 1^\circ$ in a relative humidity range of 30–90%. This is in agreement with previous results by Holysz et al. [77] in the same relative

humidity range, and can be easily understood considering that silicon wafers are polar and hydrophilic at room temperature. Similar values were also found by Zdziennicka et al. [78] for the contact angle of water on quartz, which confirms the importance of the polarity and hydrophilic character of the substrate on the water contact angle, and in particular, the density of oxygen groups. The wetting behavior of the mixtures on the silicon wafer was also found to be independent of the relative humidity (see Figure 5a,b), within the 2% uncertainty of the technique. The wetting behavior of the mixtures with the lowest surfactant concentrations was found to be the same as that of pure water. This region corresponds to the surface tension plateau found in the equilibrium adsorption isotherms of the mixtures (see Figure 4), for which the surface tensions of the mixtures were close to that of pure water. Beyond this region, a decrease in θ_a was observed along with the increase in the surfactant concentration, which corresponds to the region of decreasing surface tension. The decrease in θ_a is steeper for the PDADMAC–SLES mixtures than for the PDADMAC–SLMT ones, as is also the case for the surface tension dependences of the liquid/vapor interface. This reflects the role of liquid/vapor interfacial tension γ in the wetting behavior of these mixtures. Finally, a lower slope of θ_a dependence on the surfactant concentration region is observed at higher SLES concentration, which corresponds to the critical micellar concentration of the mixture. However, such a plateau does not exist in the PDADMAC–SLMT mixtures. The understanding of the different wetting behaviors requires a theoretical analysis of the advancing contact angle data, as well as the liquid/vapor and solid/liquid interfacial adsorption data, since the adsorption kinetics can compete with the spreading and/or evaporation kinetics.

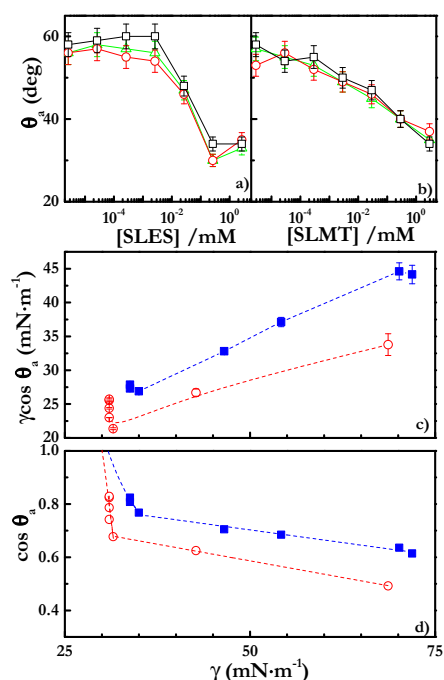


Figure 5. (a) Surfactant concentration dependences of the advancing contact angle θ_a of sessile droplets of PDADMAC–SLES mixtures with a fixed polymer concentration of 5 g/L on the silicon wafer at three different relative humidities: (Δ) 30%, (\circ) 60% and (\square) 90%. (b) Surfactant concentration dependences of the advancing contact angle θ_a of sessile droplets of PDADMAC–SLMT mixtures with a fixed polymer concentration of 5 g/L on the silicon wafer at three different relative humidities: (Δ) 30%, (\circ) 60% and (\square) 90%. (c) Representation $\gamma \cos \theta_a$ vs. γ for PDADMAC–SLMT (\blacksquare) and PDADMAC–SLES (\circ) mixtures with a fixed polymer concentration of 5 g/L. (d) $\cos \theta_a$ for PDADMAC–SLMT (\blacksquare) and PDADMAC–SLES (\circ) mixtures with a fixed polymer concentration of 5 g/L on the silicon wafer vs. equilibrium liquid/vapor interfacial tension γ . Lines are intended to act as guides.

PDADMAC–SLES mixtures displayed better surface wetting behavior than the PDADMAC–SLMT mixtures, as is evidenced from the slopes of the different regions of the plots shown in Figure 5a,b. To gain better insights into the wetting behavior of surfactant solutions and mixtures, plots of the adhesion tension have been used to provide a phenomenological correlation between θ_a and surfactant adsorption in the three-phase region [79–81].

The changes in slope in Figure 5b,c deserve a detailed discussion. It is well known that [82]

$$\frac{\partial(\gamma \cos \theta_a)}{\partial \gamma} = \frac{\Gamma_{sv} - \Gamma_{sl}}{\Gamma_{lv}}, \quad (4)$$

where Γ_{ij} is the surface excess concentration of the surfactant at the various interfaces. For pure liquids, a slope of -1 is usually obtained, while for most surfactant solutions, specific adsorption effects result in deviations from that value [79,81]. It has been frequently assumed that for solutions of non-volatile compounds, e.g., most surfactants and polymers, $\Gamma_{sv} = 0$ [83,84], thus leading to a negative value of the l.h.s. of Equation (4). This is only observed for a few points in Figure 5c, at the lowest values of the surface tension, i.e., the highest surfactant concentrations corresponding to the CMC of the surfactant solutions, where the liquid/vapor interface is saturated. For lower surfactant concentrations a positive slope is observed, thus indicating that some of the assumptions made are not correct. First, let us discuss the l.h.s. term. The γ values correspond to equilibrium ones because care has been taken to avoid evaporation. However, the results taken for θ correspond to those for which the spreading starts to overlap with the beginning of the first evaporation stage, and it is not possible to ensure that there is no overlapping between the two processes, except for non-volatile solutions. Furthermore, the spherical-cap shape of the drops was assumed for the ADSA analysis of the drop profile. The latter is a simplification, as discussed by Starov and Velarde [40]. A simplified picture of the real situation is depicted in Figure 6, where a change of curvature exists near the so-called three-phase contact line. This region is ignored when the spherical cap shape is assumed, however, from the experimental point of view it is extremely difficult to measure it due to its height. Indeed, a further complication is found in this region in the form of the domination of Derjaguin forces. This means that the real value of θ is smaller than the one measured, at least for partially wetted surfaces (see e.g., Chapter 3 in Ref. [40]). It is expected that the ignored region will be smaller as θ decreases, i.e., as γ decreases and, therefore, the experimental value of the l.h.s. calculated from the present experiments is more precise. How does the above affect the r.h.s. of Equation (3)? Assuming a spherical cap shape part of the real Γ_{sl} and Γ_{lv} values are ignored, thus assuming $\Gamma_{sv} = 0$ is not correct, except for the lowest values of γ , where the ignored volume of the drop is the smallest. This can explain the existence of a change in the slope observed in Figure 5c because the experimental data can only be explained with an effective $\Gamma_{sv} \neq 0$ [85].

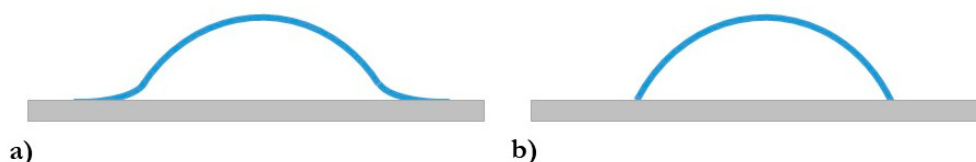


Figure 6. Sketch of the expected situation for a droplet during the spreading (a) and the idealized picture of such droplet considering the spherical cap approach (b). Notice that the definition of the true contact angle is very different in both cases.

Figure 7 shows for a better understanding as an example of the temporal evolution of the contact angle together with the adsorption kinetics at the solid/liquid interface as the temporal evolution of the surface excess obtained using the QCM-D. From the results it is clear that adsorption of surface active species should be expected during the first seconds after the deposition of the droplet on the silicon wafer, with this adsorption process

involving a time-scale slightly larger than that corresponding to the spreading. Therefore, this adsorption, and consequently the modification of the nature of the substrate, will contribute to the modification of the advancing contact angle with the surfactant concentration change. Furthermore, this may contribute to the two different wetting regions appearing as functions of the surfactant concentration. At low surfactant concentrations, the adsorption of PDADMAC–surfactant complexes onto the silicon is rather limited, and consequently, the advancing contact angle remains very close to that corresponding to the water. In contrast, the advancing contact angle decreases at the highest surfactant concentrations, in accordance with the expected increase in the deposition of polyelectrolyte–surfactant complexes [28,29].

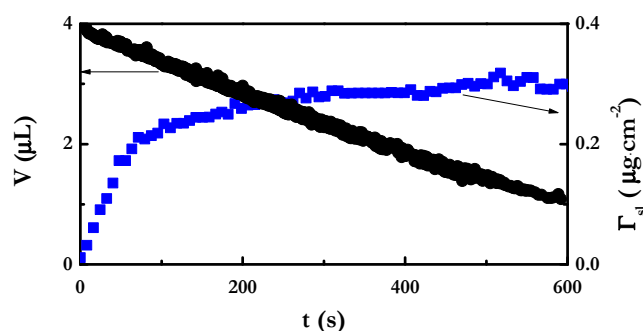


Figure 7. Time dependences of the volume of an evaporating sessile droplet at a relative humidity of 60% on a silicon wafer and of the surface excess at the solid/liquid interface, as was obtained using a quartz crystal microbalance with dissipation monitoring (QCM-D) for a PDADMAC–SLES mixture ((SLES) = 2.62 μM), with the PDADMAC concentration being 5 g/L.

Figure 5d shows the relationship between $\cos \theta_a$ and γ for the two mixtures, where two different wetting regimes are observed. The transitions in each plot occurred at different γ 's, in agreement with Zisman [86], who stated that for solutions of wetting agents the observed discontinuity in the $\cos \theta_a$ vs. γ plots depends on the nature of the wetting agent and not on the solid substrate. Figure 5c shows that the mixtures present a typical Zisman plot at low values of γ because, despite the fact that both the liquid/vapor and solid/vapor interfaces are already saturated by polyelectrolyte–surfactant complexes, the formation of the rim leads to values of θ_a that do not comply with the traditional Young equation in the high γ range. Extrapolating to $\cos \theta_a = 1$ led to a critical surface tension γ_c of the silicon wafer $31 \pm 2^\circ$, in agreement with the value obtained by Extrand and Kumagai [87]. Hence, one can argue that the use of the equilibrium liquid/vapor surface tension values of the mixtures in Figure 5c is justified.

The wetting behavior of the mixtures can be also explained in terms of the slope of the plots in Figure 5d. For surfactant solutions and mixtures, the slope of the $\cos \theta_a$ vs. γ , which represents the ratio of Γ_{sl}/Γ_{lv} , is well below unity. A higher slope means a higher tendency of transfer of surfactant molecules to the solid/liquid interface relative to the liquid/vapor interface and a better wetting behavior. The estimated slopes in both wetting regimes were higher for the PDADMAC–SLES mixtures, and therefore, the PDADMAC–SLES mixtures are more efficient wetting agents than the PDADMAC–SLMT mixtures, which is in agreement with the higher hydrophilicity of SLES. Accordingly, from a thermodynamic point view, there is a higher likelihood for the specific adsorption of the more hydrophilic molecule onto the polar substrate due to the interaction of the ethoxy groups with the silanol groups of the substrate. In addition, there is a higher tendency for the SLES molecules to spread at the liquid/vapor interface on adsorption from the mixture, as was deduced from the adsorption kinetics measurements. The motion of the SLES molecules most likely generates a Marangoni flow at the liquid/vapor interface, which ultimately resulted in the better wetting behavior observed with PDADMAC–SLES mixtures. Better spreading is useful in capillary cosmetics as it improves the coating of

complex substrates such as hair fibers, whose surface has a large number of scales that must be coated by the conditioners containing the mixtures of polyelectrolytes and surfactants.

4.4. Evaporation Behavior

4.4.1. Kinetics of Evaporation of the Mixtures

It should be noted that the evaporation process does not occur on a droplet deposited on a bare silicon wafer because, as shown above, at least partial coating of the surface takes place due to the adsorption of PDADMAC–surfactant complexes. The transport of molecules from the liquid to the vapor and the subsequent diffusion away from the liquid/air interface results in a non-uniform distribution of the evaporative flux, the maximum of which is located at the three-phase contact line (TPCL) [88–90]. In polyelectrolyte–surfactant mixtures, this results in an inhomogeneous distribution of components in the droplet, arising from surface tension gradients, with this effect being a solutal Marangoni flow directed towards or away from the TPCL. The transport of PDADMAC–surfactant complexes towards the TPCL, and the subsequent adsorption onto the substrate, leads to the pinning of the contact lines [90]. The evaporation behavior of solutions and complex fluids has been analyzed in terms of the time evolution of θ and L [91,92]. For the sake of example, Figure 8a shows the results for the PDADMAC–SLES mixture ((SLES) = 2.62 μM) at a relative humidity of 60%. The initial spreading was also monitored.

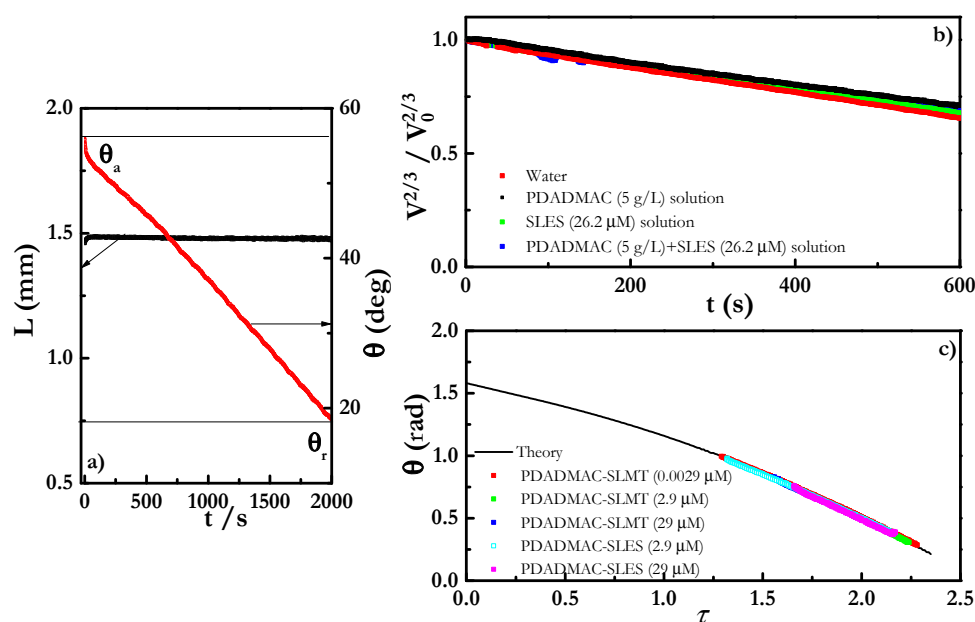


Figure 8. (a) Time dependence of the contact angle θ and the contact length L for a sessile droplet of PDADMAC–SLES mixture ((SLES) = 2.62 μM) during evaporation on a silicon wafer at relative humidity of 60%. (b) Plots of $V^{2/3}/V_0^{2/3}$ vs. time for evaporating a sessile droplet on a silicon wafer at a relative humidity of 60%. (c) Dependence of the contact angle θ on the dimensionless time $\tilde{\tau}$ for the evaporation of different polyelectrolyte–surfactant mixtures, with a PDADMAC concentration of 5 g/L, at a relative humidity of 60%. The solid line is the theoretical solution to the equation for the first evaporation stage, obtained according to Semenov et al. [39].

It is observed that L remained constant, while θ decreased continuously with time for the whole duration of evaporation. The constant contact length might be due to the pinning of the droplet on the silicon wafer as a result of the deposition of PDADMAC, SLES and PDADMAC–SLES complexes at the TPCL. This is supported by the appreciable level of adsorption at the solid/liquid interface that occurred during the spreading stage. The solutal Marangoni flow within the evaporating droplet drags poly(diallyldimethylammonium) and Laureth sulfate ions towards its perimeter, thus leading to an increased concentration of these ions near the droplet edge, followed by their eventual deposition. The idea of

solvent transfer leading to pinned contact lines has been discussed by Deegan et al. [93], who studied evaporating droplets of suspensions of polystyrene.

A similar evaporation process to that shown in Figure 8a was also found at relative humidity values of 30 and 90%, with the only difference being the evaporation times of the droplets. In essence, the evaporation rate of the mixture on the silicon wafer varies with the water content of the surrounding vapor, while the process of evaporation remained qualitatively unchanged. Furthermore, the trends in the relative humidity dependence of the evaporation rate and the time evolutions of θ and L were similar for the PDADMAC–SLES mixtures and the PDADMAC–SLMT mixtures at all the surfactant concentrations studied.

The effect of the adsorbed layers on the evaporation rate can be discussed in terms of the work by Doganci et al. [23], as detailed in Appendix B. A comparison of the time dependences of the relative volume of the evaporating sessile droplets for a PDADMAC–SLES mixture, a SLES solution, a PDADMAC solution and pure water is shown in Figure 8b. The estimated slopes of the plots were the same within an experimental error of 5%, which gives an indication of the similarity between the evaporation rates of pure water and those of the mixtures and solutions. The reason for this similarity in the evaporation rates of water from the surface containing an adsorbed layer and that of pure water is due to the location of the adsorption layer. Moroi et al. [94] pointed out the existence of a finite layer of water molecules between the adsorbed monolayers of surfactants and the liquid/vapor interface and that water molecules move faster than the surfactant molecules. Lunkenheimer and Zembala [95] also found that evaporation retardation only takes place at high surfactant concentrations. Thus, it may be assumed that during the first stage of the evaporation the results of θ and L can be described by universal curves. Therefore, according to Doganci et al. [23], in addition to the results in Figure 8b, it appears clear that the presence of monolayers does not quantitatively modify the evaporation rate, which makes it reasonable to check whether the theory is able to describe the present results.

4.4.2. Theoretical Analysis of Evaporation of the Mixtures

The reduced time $\tilde{\tau}$ is defined in detail in Appendix A. Briefly, $\tilde{\tau} = t/t_{ch}$, with t_{ch} being a characteristic time given by $t_{ch} = L^2/\beta$. β is a function of θ and its time derivative. The key result of this theory is that, while the θ vs. t curves depend on the nature of the fluid and of the solid substrate, the θ vs. $\tilde{\tau}$ curve is universal. The comparison of the theoretical behavior and the experimental evaporation data for the mixtures is shown in Figure 8c, where a very good agreement between the evaporation behavior of the mixtures and the theoretical prediction is observed. It should be pointed out that this agreement is universal irrespective of the humidity condition. The theoretical description of the first stage of evaporation, as summarized by Semenov et al. [39], has been shown to sufficiently explain the evaporation behaviors of pure liquid [18,39], micro- and nano-suspensions [18,93] and surfactant solutions [19] on solid substrates. The agreement for complex fluids is rather surprising due to the competition between the evaporation kinetics and the adsorption kinetics at the liquid/vapour and the solid/liquid interfaces [96].

For the mixtures in the present study, adsorption at both interfaces and the change in polymer and surfactant concentration during the evaporation process led to the time dependence of the surface tension at both interfaces, which according to Young's equation, modifies the contact angle. Interestingly, these time dependence effects were not taken into account in the formulation of the theory, giving an indication that the behavior of liquids in the first stage evaporation is independent of the nature of the liquid or the solid substrate. Finally, it is worthwhile to point out that the same conclusion was obtained for trisiloxanes and sodium dodecylsulfate solutions [19,97].

5. Conclusions

The wetting and evaporation behaviors of PDADMAC–SLMT and PDADMAC–SLES aqueous mixtures on silicon wafers was studied in terms of the changes of the advancing

contact angles θ_a of sessile droplets of the mixtures on a solid substrate during the spreading and evaporation of the solution.

The wetting of polyelectrolyte–surfactant mixtures has been found to be independent of the environmental humidity, and dependent on the nature and concentration of the surfactant. This seems to be reasonable considering the differences on the physico-chemical properties of the complexes formed in the bulk and the characteristics of the adsorption layers formed at liquid/vapor and solid/liquid interfaces. Thus, PDADMAC–SLES mixtures have provided evidence for the superior wetting behavior compared to those containing SLMT. This is the result of enhanced adsorption at the solid/liquid interface of mixtures containing SLES, as evidenced by the surfactant concentration dependence of θ_a plots and the $\cos \theta_a$ vs. γ plots. This is explained considering a higher hydrophilic nature of the SLES molecule, which may favor its adsorption at the polar silicon wafer surface, and from the ability of PDADMAC–SLES complexes to dissociate upon adsorption at the liquid/vapor interface. The latter is associated with a solutal Marangoni flow controlling the enhanced wetting behavior of PDADMAC–SLES mixtures.

On the other hand, the evaporation of the mixtures—appearing as independent of the surfactant concentration and the relative humidity—was found to occur in a single stage. This may result from the pinning of the TPCL due to the deposition of the constituents of the mixtures at the perimeter of the droplets. The adsorption of surface layers at the liquid/vapor interface does not affect the evaporation rate in relation to that of pure water, which may be rationalized by the existence of a finite layer of water molecules between the free liquid/vapor surface and the monolayer. Furthermore, the evaporation of the studied mixtures is well described in terms of the universal law accounting for the evaporation of pure fluid droplets.

It should be noted that this theoretical description, accounting for the changes of the contact angle during the evaporation, is an oversimplified picture of the real situation that occurs in solutions of surface active compounds. This is because the temporal evolution of the contact angle is coupled to two concurrent processes acting in different directions: (i) reduction in the liquid volume due to the evaporation (increase in the solution concentration), and (ii) depletion of material from the solution due to the adsorption of surface active compounds (polymer, surfactant and their complexes) to the liquid/solid and liquid/vapor interfaces. Consequently, it is necessary to refine the theoretical model used for the description of evaporation, in order to account for the change in the concentration of the solution, i.e., $\theta = f(t, c(t))$. An initial approach to address the impact of the changes in the solution concentration, as result of the abovementioned concurrent processes, is discussed in Appendix C.

Author Contributions: Conceptualization, L.P. and R.G.R.; methodology, A.A. and L.P.; software, A.A., L.P. and E.G.; validation, L.P. and R.G.R.; formal analysis, L.P.; investigation, A.A., L.P., E.G., S.L., V.M.S., F.O., R.G.R. and M.G.V.; resources, F.O., R.G.R. and M.G.V.; data curation, L.P. and R.G.R.; writing—original draft preparation, A.A., L.P., E.G. and R.G.R.; writing—review and editing, L.P., E.G., V.M.S., F.O., R.G.R. and M.G.V.; visualization, E.G.; supervision, R.G.R. and M.G.V.; project administration, R.G.R.; funding acquisition, E.G., F.O., R.G.R. and M.G.V. All authors have read and agreed to the published version of the manuscript.

Funding: This work was funded in part by MINECO (Spain) under grants CTQ2016-78895-R and PID2019-106557GB-C21, by Banco Santander-Universidad Complutense grant PR87/19-22513 (Spain) and by E.U. on the framework of the European Innovative Training Network-Marie Skłodowska-Curie Action NanoPaint (grant agreement 955612).

Data Availability Statement: Data available on request.

Acknowledgments: We are grateful to the Centro de Espectroscopía y Correlación of Complutense University of Madrid for the use of some of its facilities.

Conflicts of Interest: The authors declare no conflict of interest. The funders had no role in the design of the study; in the collection, analyses, or interpretation of data; in the writing of the manuscript, or in the decision to publish the results.

Appendix A. Theoretical Description of the Evaporation

The theoretical description of the first two stages of the evaporation requires making two main assumptions: (i) droplets maintain a spherical-cap shape during the process, and (ii) the evaporation is a diffusion limited process when droplets present a diameter of their base above 1 μm [61]. This leads to a droplet volume V , which can be defined as

$$V = L^3 f(\theta) \quad (\text{A1})$$

where $f(\theta) = \frac{\pi}{3} \frac{(1-\cos\theta)^2(2+\cos\theta)}{\sin^3\theta}$ and L is the contact length. The evaporation rate for a sessile drop can be defined as follows [98,99]

$$\frac{dV}{dt} = -2\pi \frac{DM}{\rho} [C_{sat}(T_{surf}) - HC_{sat}(T_\infty)] F(\theta)L \quad (\text{A2})$$

where V is the drop volume, t is the time, D , ρ and M are vapor diffusivity in the air, density of the liquid and its molar mass, respectively; H and T_∞ are the humidity and temperature of the ambient air, respectively; T_{surf} is the temperature of the droplet–air interface; $C_{sat}(T_{surf})$ and $C_{sat}(T_\infty)$ are the molar concentrations of the saturated vapor at the corresponding temperatures; $F(\theta)$ is a function of the contact angle which will be described below. On the basis of the above definition, Equation (A2) can be rewritten as [19,100]

$$\frac{dV}{dt} = -\beta F(\theta)L \quad (\text{A3})$$

where $\beta = 2\pi \frac{DM}{\rho} (C_{sat}(T_{av}) - C_\infty)$ is a parameter that depends on the average temperature, T_{av} , of the droplet surface and C_∞ is the molar concentration of the vapor in the ambient air far away from the droplet. Assuming a constant value for T_{av} , it is possible to assume that the parameter β is also constant. Hence, the expressions for the stages of evaporation can be deduced [39], with $F(\theta)$ being approximated by

$$F(\theta) \begin{cases} (0.6366\theta + 0.09591\theta^2 - 0.06194\theta^3)/\sin\theta & \theta < \pi/18 \\ (0.00008957 + 0.6366\theta + 0.116\theta^2 - 0.08878\theta^3 + 0.01033\theta^4)/\sin\theta & \theta > \pi/18 \end{cases} \quad (\text{A4})$$

Experimental limitations only allow the observation of the constant contact radius stage during the experiments. As will be shown below, the formation of a rim at the phase contact line that pins it does not allow for maintenance of the spherical-cap shape, or to accurately measure the height of the droplet.

Given that the contact radius ($L/2$) remains constant during the first stage of the evaporation, Equation (3) can be rewritten as

$$L^3 f'(\theta)(d\theta/dt) = -\beta F(\theta)L \quad (\text{A5})$$

thus,

$$L^2 f'(\theta) \left(\frac{d\theta}{dt} \right) = -\beta F(\theta) \quad (\text{A6})$$

Introducing a dimensionless time $\tau = t/t_{ch}$, with t_{ch} being a characteristic time of the process given as L^2/β , it is possible to rewrite Equation (A6) as follows

$$f'(\theta) \left(\frac{d\theta}{d\tau} \right) = -F(\theta) \quad (\text{A7})$$

The direct integration of Equation (A8) with the corresponding boundary conditions yields

$$A(\theta, \theta_a) = \tau \quad (\text{A8})$$

where $(\theta, \theta_a) = \int_{\theta}^{\theta_a} (f(\theta)/F(\theta))d\theta$, with θ being the advancing contact angle θ_a at $t = 0$ (in the absence of spreading). Equation (A8) indicates that the deduced relationship should be universal and not dependent on the liquid nature or the droplet volume, and the only parameter to be determined from the experiment is the advancing contact angle. Finally, the first stage of evaporation should proceed until the contact angle reaches the receding contact angle θ_r , and as such, it can be concluded from Equation (A8) that $A(\theta_r, \theta_a) = \tau$, will signify the end of the first stage of evaporation.

Appendix B. Adsorbed Surface Layers and Evaporation Rate

It is frequently assumed that the adsorbed layer at the liquid/vapor interface slows down the evaporation rate of water. However, Moroi et al. [95] showed that the adsorbed monolayers of surfactants do not provide any additional barrier to the evaporation of water, at least for the first evaporation stage and low surfactant concentrations. In the present study, the comparison between the evaporation rates of pure water and that of the mixture was guided by the work of Doganci et al. [98]. Assuming that the rate of volume change of the sessile droplet, i.e., its evaporation rate, is diffusion-controlled, the authors derived the equation

$$\frac{V^{2/3}}{V_0^{2/3}} = 1 - \frac{2K_w}{3V_0^{2/3}}f(\theta)t, \quad (\text{A9})$$

where V_0 and V are the initial volume of the sessile droplet and its instantaneous volume at a given time t , respectively. The quantity $f(\theta)$ is almost constant although a small variation may be expected when different substrates are compared [93]. Furthermore, given that $K_w = \frac{4D\pi^{(2/3)}3^{(1/3)}(c_0 - c_\infty)}{\rho_L(2 - 3\cos\theta + \cos^3\theta)^{(1/3)}}$, the slope of the plot $V^{2/3}/V_0^{2/3}$ vs. t should give an indication of the evaporation rate of the liquid. In the above expression D is the diffusion coefficient of the vapor, ρ_L is the liquid density, c_0 and c_∞ are the vapor concentration at the droplet surface and at an infinite distance from the droplet surface, respectively, one would expect that K_w is a constant and that depends mainly on the properties of the vapor.

Appendix C. Effect of the Change of the Solution Concentration on the Contact Angle during the Evaporation

The theoretical description of evaporation introduced in Appendices A and B does not account for any change in the solution concentration, or as result of the volume reduction occurring during evaporation or due to the depletion of surface active species as result of the adsorption to the solution/vapor and solution/solid interface. This is important because it is well-known that polyelectrolyte–surfactant complexes formed in solution can adsorb to both the liquid/air and liquid/solid interfaces, which is expected to decrease the concentration of the solution [28,45]. Moreover, the adsorption will also modify the interfacial tensions. On the other side, the evaporation is associated with a decrease in the droplet volume, which is associated as matter of fact with an increase in the solution concentration. Therefore, the competition of the adsorption at the interfaces and the evaporation, modify the real concentration of the evaporating droplet, and hence, these aspects should be included in any comprehensive model describing the evaporation of droplets containing surface active compounds, i.e., the contact angle should be described as $\theta = f(t, c(t))$. Below, the effect of the change in concentration as function of the change in adsorbed amount at the water/vapor and water/solid interface and the evaporation is discussed. Figure A1 displays the typical behavior of the three kinetic processes, i.e., contact angle change, adsorption at the liquid/vapor interface as the dynamic surface tension, and adsorption at the liquid/solid interface as the time evolution of the surface excess, competing during the spreading and evaporation of the solution droplet.

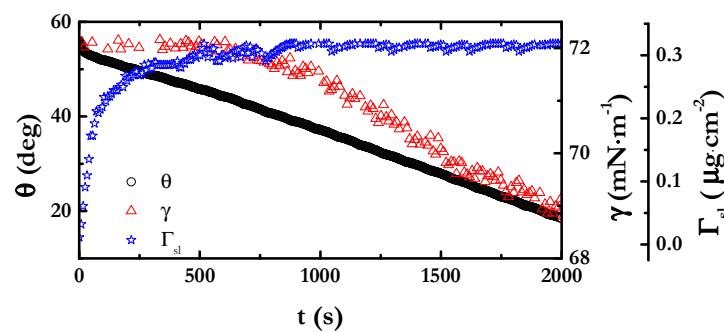


Figure A1. Time dependences of the contact angle θ of a sessile droplet of a PDADMAC–SLES mixture during evaporation on a silicon wafer at relative humidity of 60%, the surface tension of the liquid/vapor interface γ during the adsorption of a PDADMAC–SLES mixture and the surface excess of the solid/liquid interface during the adsorption of a PDADMAC–SLES mixture. The three experiments correspond to a PDADMAC–SLES mixture with a PDADMAC concentration of 5 g/L and (SLES) = 2.62 μM .

The droplet volume remains constant during the first seconds after the deposition on the silicon wafer of a droplet with an aqueous solution of concentration c_0 , and hence, no concentration change associated with the droplet volume should be expected during the spreading stage. However, from the results shown in Figure A1, it is clear that from the initial time t_0 there is a depletion of surface active species from the solution to the solid/liquid interface, i.e., Γ_{sl} increases. This will reduce the real solution concentration (notice that here that only the results for PDADMAC–SLES mixtures are shown, for results on PDADMAC–SLMT, see our previous paper [28]). Furthermore, even for the case of the PDADMA–SLES mixture it appears that for a short surfactant concentration induction time, a certain depletion of surface active species as a result of the adsorption at the liquid/vapor interface may also be expected. Consequently, the concentration of the droplet when the first stage of the evaporation starts, t_1 , may be defined as follows

$$c_1 = c_0 - c_{sl}(t_1) - c_{lv}(t_1) \quad (\text{A10})$$

with $c_{sl}(t_1)$ and $c_{lv}(t_1)$ being the depleted concentrations for adsorption to the solid/liquid and liquid/vapor interfaces at the end of the spreading stage, respectively. During the evaporation, i.e., $t > t_1$, there is a decrease in the droplet volume, which can be defined in terms of the between the concentration at a time t ($c(t)$) and the concentration when the evaporation starts (c_1), given as follows

$$\frac{V(t)}{V_0} = \frac{c_1}{c(t)} \quad (\text{A11})$$

and consequently, the time dependence of the concentration may be defined during the evaporation process according to the following expression

$$c(t) = \frac{V_0}{V(t)} c_1 \quad (\text{A12})$$

Equation (A12) presents an interesting approach for evaluating the concentration of the evaporating droplet. However, the increase in the concentration associated with the evaporation also modifies the depleted amount for adsorption to the liquid/solid and liquid/vapor interfaces. This is clear from Figure A2, where the surface excesses of the liquid/solid interface for different SLES concentrations are shown. It should be noted that a qualitatively similar dependence should be expected for the adsorption to the liquid/vapor interface.

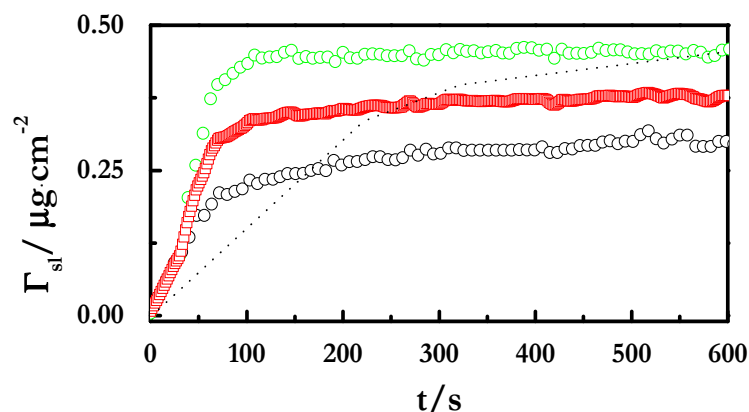


Figure A2. Time dependence of the surface excess at the solid/liquid interface, as was obtained using a quartz crystal microbalance for the adsorption of PDADMAC–SLES mixtures with three different concentrations (o (SLES) = 2.62 μM , o (SLES) = 15 μM and o (SLES) = 2.62 mM) on a silicon wafer and PDADMAC concentration of 5 g/L. The dotted black line corresponds to the hypothetical surface excess corresponding to the adsorption of an evaporating droplet with an initial [SLES] = 2.62 μM .

The change in the volume, and the consequent increase in the solution concentrations, should result in a progressive increase in the surface excess at the solid/liquid as indicated by the dotted line in Figure A2. A similar trend may be expected for the liquid/vapor interface, considering the time evolution of the surface tension and its correlation with the surface excess, which can be defined in the simplest way assuming a pseudo-binary system for the Gibbs equation $\Gamma_{lv} = -\frac{1}{RT} \left(\frac{\partial \gamma(t)}{\partial \ln c(t)} \right)$, with R and T being the gas constant and the absolute temperature. Thus, it is possible to define the effective concentration of the droplet for any time t during the evaporation process as

$$c(t) = \frac{V_0}{V(t)} c_1 - c_{sl}(t) - c_{lv}(t), \quad (\text{A13})$$

where $c_{sl}(t)$ and $c_{lv}(t)$ correspond to the depleted concentrations for adsorption to the solid/liquid and liquid/vapor interfaces for $t > t_1$, respectively. It is worth mentioning that even the determination of the surface excesses of both interfaces requires additional work. It is possible to determine the surface excess of the solid/liquid interface using ellipsometry, QCM-D, surface plasmon resonance or neutron reflectometry, and the corresponding liquid/vapor interface using neutron reflectometry or the Gibbs equation assuming a pseudo-binary system (valid for $c_0 < \text{critical micelle concentration}$).

The above discussion evidences that the concentration changes during the evaporation of the droplet, and hence, it is necessary to redefine the time evolution of the contact angle. Thus, assuming that $\Gamma_{sv} \approx 0$, and the Equation (3) is fulfilled for any value of the contact angle, it is possible to write the following expression

$$\frac{\partial(\gamma \cos \theta)}{\partial \gamma} \approx -\frac{\Gamma_{sl}}{\Gamma_{lv}}. \quad (\text{A14})$$

Both Γ_{sl} and Γ_{lv} , and the surface tension γ are dependent on the concentration and time, and hence, it is necessary to introduce such dependence. Thus, Equation (A14) should read

$$\frac{\partial(\gamma \cos \theta)}{\partial \gamma(c(t))} \approx -\frac{\Gamma_{sl}(c(t))}{\Gamma_{lv}(c(t))} \quad (\text{A15})$$

which may be rewritten as

$$\int_{c(t_1)}^{c(t)} d(\gamma \cos \theta) = - \int_{\gamma(c(t_1))}^{\gamma(c(t))} \frac{\Gamma_{sl}(c(t))}{\Gamma_{lv}(c(t))} d\gamma(c(t)) \quad (\text{A16})$$

Integrating Equation (A16), the dependence of the contact angle on the instantaneous concentration during the first evaporation step may be obtained

$$\gamma(c(t)) \cos \theta(c(t)) - \gamma(c(t_1)) \cos \theta(c(t_1)) = - \int_{\gamma(c(t_1))}^{\gamma(c(t))} \frac{\Gamma_{sl}(c(t))}{\Gamma_{lv}(c(t))} d\gamma(c(t)) \quad (\text{A17})$$

and thus, reorganizing Equation (A17) and substituting $\cos \theta(c(t_1))$ for its value ($\cos \theta_a$), the function $\theta = f(t, c(t))$ is obtained

$$\cos \theta(c(t)) = \frac{\gamma(c_1) \cos \theta_a}{\gamma(c(t))} - \frac{1}{\gamma(c(t))} \int_{\gamma(c(t_1))}^{\gamma(c(t))} \frac{\Gamma_{sl}(c(t))}{\Gamma_{lv}(c(t))} d\gamma(c(t)) \quad (\text{A18})$$

References

- Diddens, C.; Tan, H.; Lv, P.; Versluis, M.; Kuerten, J.G.M.; Zhang, X.; Lohse, D. Evaporating pure, binary and ternary droplets: Thermal effects and axial symmetry breaking. *J. Fluid Mech.* **2017**, *823*, 470–497. [CrossRef]
- Worden, J.; Noone, D.; Bowman, K. Importance of rain evaporation and continental convection in the tropical water cycle. *Nature* **2007**, *445*, 528–532. [CrossRef]
- Fakhru'l-Razi, A.; Pendashteh, A.; Abdullah, L.C.; Biak, D.R.A.; Madaeni, S.S.; Abidin, Z.Z. Review of technologies for oil and gas produced water treatment. *J. Hazard. Mat.* **2009**, *170*, 530–551. [CrossRef] [PubMed]
- Kitano, T.; Nishio, J.; Kurose, R.; Komori, S. Evaporation and combustion of multicomponent fuel droplets. *Fuel* **2014**, *136*, 219–225. [CrossRef]
- Perrin, L.; Castanet, G.; Lemoine, F. Characterization of the evaporation of interacting droplets using combined optical techniques. *Exp. Fluids* **2015**, *56*, 29. [CrossRef]
- Duan, F.; Ward, C.A. Investigation of Local Evaporation Flux and Vapor-Phase Pressure at an Evaporative Droplet Interface. *Langmuir* **2009**, *25*, 7424–7431. [CrossRef] [PubMed]
- He, C.; Liu, C.; Gao, H.; Xie, H.; Li, Y.; Wu, S.; Xu, J. The optimal evaporation temperature and working fluids for subcritical organic Rankine cycle. *Energy* **2012**, *38*, 136–143. [CrossRef]
- Günay, A.A.; Sett, S.; Oh, J.; Miljkovic, N. Steady Method for the Analysis of Evaporation Dynamics. *Langmuir* **2017**, *33*, 12007–12015. [CrossRef]
- Sáenz, P.J.; Wray, A.W.; Che, Z.; Matar, O.K.; Valluri, P.; Kim, J.; Sefiane, K. Dynamics and universal scaling law in geometrically-controlled sessile drop evaporation. *Nature Comm.* **2017**, *8*, 14783. [CrossRef]
- Tan, H.; Diddens, C.; Lv, P.; Kuerten, J.G.M.; Zhang, X.; Lohse, D. Evaporation-triggered microdroplet nucleation and the four life phases of an evaporating Ouzo drop. *Proc. Nat. Acad. Sci. USA* **2016**, *113*, 8642–8647. [CrossRef] [PubMed]
- Sobac, B.; Brutin, D. Thermocapillary instabilities in an evaporating drop deposited onto a heated substrate. *Phys. Fluids* **2012**, *24*, 032103. [CrossRef]
- Gao, M.; Kong, P.; Zhang, L.-X. Evaporation dynamics of different sizes sessile droplets on hydrophilic and hydrophobic heating surface under constant wall heat fluxes conditions. *Int. Comm. Heat Mass Transf.* **2018**, *93*, 93–99. [CrossRef]
- Christy, J.R.E.; Sefiane, K.; Munro, E. A Study of the Velocity Field during Evaporation of Sessile Water and Water/Ethanol Drops. *J. Bionic Eng.* **2010**, *7*, 321–328. [CrossRef]
- He, M.; Qiu, H. Internal flow patterns of an evaporating multicomponent droplet on a flat surface. *Int. J. Therm. Sci.* **2016**, *100*, 10–19. [CrossRef]
- Shi, L.; Shen, P.; Zhang, D.; Lin, Q.; Jiang, Q. Wetting and evaporation behaviors of water–ethanol sessile drops on PTFE surfaces. *Surf. Interface Anal.* **2009**, *41*, 951–955. [CrossRef]
- Guéna, G.; Poulard, C.; Cazabat, A.M. Evaporating drops of alkane mixtures. *Colloids Surf. A* **2007**, *298*, 2–11. [CrossRef]
- Báez-López, D.; Báez-Villegas, D.A. *Matlab Handbook with Applications to Mathematics, Engineering and Finance*; Chapman and Hall/CRC: Boca Raton, FL, USA, 2019.
- Perrin, L.; Pajor-Swierzy, A.; Magdassi, S.; Kamysnyy, A.; Ortega, F.; Rubio, R.G. Evaporation of Nanosuspensions on Substrates with Different Hydrophobicity. *ACS Appl. Mat. Interfaces* **2018**, *10*, 3082–3093. [CrossRef]

19. Semenov, S.; Trybala, A.; Agogo, H.; Kovalchuk, N.; Ortega, F.; Rubio, R.G.; Starov, V.M.; Velarde, M.G. Evaporation of droplets of surfactant solutions. *Langmuir* **2013**, *29*, 10028–10036. [[CrossRef](#)]
20. Pham, T.; Kumar, S. Drying of Droplets of Colloidal Suspensions on Rough Substrates. *Langmuir* **2017**, *33*, 10061–10076. [[CrossRef](#)] [[PubMed](#)]
21. Larson, R.G. Transport and deposition patterns in drying sessile droplets. *AIChE J.* **2014**, *60*, 1538–1571. [[CrossRef](#)]
22. Mampallil, D.; Eral, H.B. A review on suppression and utilization of the coffee-ring effect. *Adv. Colloid Interface Sci.* **2018**, *252*, 38–54. [[CrossRef](#)] [[PubMed](#)]
23. Armstrong, S.; McHale, G.; Ledesma-Aguilar, R.; Wells, G.G. Pinning-Free Evaporation of Sessile Droplets of Water from Solid Surfaces. *Langmuir* **2019**, *35*, 2989–2996. [[CrossRef](#)] [[PubMed](#)]
24. Vaynberg, A.; Stuart, M.; Wu, X.-F. Differential wetting characterization of hair fibers. *J. Cosmet. Sci.* **2012**, *63*, 33–41.
25. Fernández-Peña, L.; Abelenda-Nuñez, I.; Hernández-Rivas, M.; Ortega, F.; Rubio, R.G.; Guzmán, E. Impact of the bulk aggregation on the adsorption of oppositely charged polyelectrolyte-surfactant mixtures onto solid surfaces. *Adv. Colloid Interface Sci.* **2020**, *282*, 102203. [[CrossRef](#)] [[PubMed](#)]
26. Llamas, S.; Guzmán, E.; Akanno, A.; Fernández-Peña, L.; Ortega, F.; Campbell, R.A.; Miller, R.; Rubio, R.G. Study of the Liquid/Vapor Interfacial Properties of Concentrated Polyelectrolyte–Surfactant Mixtures Using Surface Tensiometry and Neutron Reflectometry: Equilibrium, Adsorption Kinetics, and Dilational Rheology. *J. Phys. Chem. C* **2018**, *122*, 4419–4427. [[CrossRef](#)]
27. Llamas, S.; Guzmán, E.; Ortega, F.; Baghdadli, N.; Cazeneuve, C.; Rubio, R.G.; Luengo, G.S. Adsorption of polyelectrolytes and polyelectrolytes-surfactant mixtures at surfaces: A physico-chemical approach to a cosmetic challenge. *Adv. Colloid Interface Sci.* **2015**, *222*, 461–487. [[CrossRef](#)] [[PubMed](#)]
28. Llamas, S.; Guzmán, E.; Baghdadli, N.; Ortega, F.; Cazeneuve, C.; Rubio, R.G.; Luengo, G.S. Adsorption of poly(diallyldimethylammonium chloride)—sodium methyl-cocoyl-taurate complexes onto solid surfaces. *Colloids Surf. A* **2016**, *505*, 150–157. [[CrossRef](#)]
29. Guzmán, E.; Llamas, S.; Fernández-Peña, L.; Léonforte, F.; Baghdadli, N.; Cazeneuve, C.; Ortega, F.; Rubio, R.G.; Luengo, G.S. Effect of a natural amphoteric surfactant in the bulk and adsorption behavior of polyelectrolyte-surfactant mixtures. *Colloids Surf. A* **2020**, *585*, 124178. [[CrossRef](#)]
30. Fernández-Peña, L.; Guzmán, E.; Leonforte, F.; Serrano-Pueyo, A.; Regulski, K.; Tournier-Couturier, L.; Ortega, F.; Rubio, R.G.; Luengo, G.S. Effect of molecular structure of eco-friendly glycolipid biosurfactants on the adsorption of hair-care conditioning polymers. *Colloids Surf. B* **2020**, *185*, 110578. [[CrossRef](#)]
31. Fernández-Peña, L.; Guzmán, E.; Ortega, F.; Bureau, L.; Leonforte, F.; Velasco, D.; Rubio, R.G.; Luengo, G.S. Physico-chemical study of polymer mixtures formed by a polycation and a zwitterionic copolymer in aqueous solution and upon adsorption onto negatively charged surfaces. *Polymer* **2021**, *217*, 123442. [[CrossRef](#)]
32. Llamas, S.; Guzmán, E.; Ortega, F.; Rubio, R.G. Adsorption of Mixtures of a Pegylated Lipid with Anionic and Zwitterionic Surfactants at Solid/Liquid. *Colloids Interfaces* **2020**, *4*, 47. [[CrossRef](#)]
33. Lindman, B.; Antunes, F.; Aidarova, S.; Miguel, M.; Nylander, T. Polyelectrolyte-surfactant association—from fundamentals to applications. *Colloid J.* **2014**, *76*, 585–594. [[CrossRef](#)]
34. Fernández-Peña, L.; Guzmán, E. Physicochemical Aspects of the Performance of Hair-Conditioning Formulations. *Cosmetics* **2020**, *7*, 26. [[CrossRef](#)]
35. Hernández-Rivas, M.; Guzmán, E.; Fernández-Peña, L.; Akanno, A.; Greaves, A.; Léonforte, F.; Ortega, F.; Rubio, R.G.; Luengo, G.S. Deposition of Synthetic and Bio-Based Polycations onto Negatively Charged Solid Surfaces: Effect of the Polymer Cationicity, Ionic Strength, and the Addition of an Anionic Surfactant. *Colloids Interfaces* **2020**, *4*, 33. [[CrossRef](#)]
36. Cheraghian, G. Evaluation of Clay and Fumed Silica Nanoparticles on Adsorption of Surfactant Polymer during Enhanced Oil Recovery. *J. Japan Petr. Inst.* **2017**, *60*, 85–94. [[CrossRef](#)]
37. Cheraghian, G. An Experimental Study of Surfactant Polymer for Enhanced Heavy Oil Recovery Using a Glass Micromodel by Adding Nanoclay. *Petr. Sci. Techn.* **2015**, *33*, 1410–1417. [[CrossRef](#)]
38. Kovalchuk, N.M.; Trybala, A.; Starov, V.M. Evaporation of sessile droplets. *Curr. Opin. Colloid Interface Sci.* **2014**, *19*, 336–342. [[CrossRef](#)]
39. Semenov, S.; Starov, V.M.; Rubio, R.G.; Agogo, H.; Velarde, M.G. Evaporation of sessile water droplets: Universal behaviour in presence of contact angle hysteresis. *Colloids Surf. A* **2011**, *391*, 135–144. [[CrossRef](#)]
40. Starov, V.M.; Velarde, M.G. *Wetting and Spreading Dynamics*; CRC Press: Boca Raton, FL, USA, 2019.
41. Semenov, S.; Trybala, A.; Rubio, R.G.; Kovalchuk, N.; Starov, V.; Velarde, M.G. Simultaneous spreading and evaporation: Recent developments. *Adv. Colloid Interface Sci.* **2014**, *206*, 382–398. [[CrossRef](#)]
42. Craster, R.V.; Matar, O.K.; Sefiane, K. Pinning, Retraction, and Terracing of Evaporating Droplets Containing Nanoparticles. *Langmuir* **2009**, *25*, 3601–3609. [[CrossRef](#)]
43. Bormashenko, E.; Musin, A.; Zinigrad, M. Evaporation of droplets on strongly and weakly pinning surfaces and dynamics of the triple line. *Colloids Surf. A* **2011**, *385*, 235–240. [[CrossRef](#)]
44. Friedrich, L.C.; Silva, V.O.; Moreira, P.F., Jr.; Tcacenco, C.M.; Quina, F.H. Time-resolved fluorescence quenching studies of sodium lauryl ether sulfate micelles. *J. Braz. Chem. Soc.* **2013**, *24*, 241–245. [[CrossRef](#)]
45. Llamas, S.; Fernández-Peña, L.; Akanno, A.; Guzmán, E.; Ortega, V.; Ortega, F.; Csaky, A.G.; Campbell, R.A.; Rubio, R.G. Towards understanding the behavior of polyelectrolyte–surfactant mixtures at the water/vapor interface closer to technologically-relevant conditions. *Phys. Chem. Chem. Phys.* **2018**, *20*, 1395–1407. [[CrossRef](#)]

46. Mostafalu, R.; Banaei, A.; Ghorban, F. An Inaccuracy in the Determination of Cocoamidopropyl Betaine by the Potentiometric Method. *J. Surfact. Deterg.* **2015**, *18*, 919–922. [[CrossRef](#)]
47. Mészáros, R.; Thompson, L.; Bos, M.; Varga, I.; Gilányi, T. Interaction of Sodium Dodecyl Sulfate with Polyethyleneimine: Surfactant-Induced Polymer Solution Colloid Dispersion Transition. *Langmuir* **2003**, *19*, 609–615. [[CrossRef](#)]
48. Mezei, A.; Pojják, K.; Mészáros, R. Nonequilibrium Features of the Association between Poly(vinylamine) and Sodium Dodecyl Sulfate: The Validity of the Colloid Dispersion Concept. *J. Phys. Chem B* **2008**, *112*, 9693–9699. [[CrossRef](#)]
49. Akanno, A.; Guzmán, E.; Fernández-Peña, L.; Llamas, S.; Ortega, F.; Rubio, R.G. Equilibration of a polycation–anionic surfactant mixture at the water/vapor interface. *Langmuir* **2018**, *34*, 7455–7464. [[CrossRef](#)] [[PubMed](#)]
50. Guzmán, E.; Fernández-Peña, L.; Akanno, A.; Llamas, S.; Ortega, F.; Rubio, R.G. Two Different Scenarios for the Equilibration of Polycation—Anionic Solutions at Water–Vapor Interfaces. *Coatings* **2019**, *9*, 438. [[CrossRef](#)]
51. Luengo, G.S.; Galliano, A.; Dubief, C. Aqueous Lubrication in Cosmetics. In *Aqueous Lubrication*; Spencer, N.D., Ed.; World Scientific Publishing Co Pte Ltd.: Singapore, 2014; pp. 103–144.
52. Gavazzoni Dias, M.F.R. Hair cosmetics: An overview. *Int. J. Trichology* **2015**, *7*, 2–15. [[CrossRef](#)]
53. Mezei, A.; Mezaros, R. Novel Method for the Estimation of the Binding Isotherms of Ionic Surfactants on Oppositely Charged Polyelectrolytes. *Langmuir* **2006**, *22*, 7148–7151. [[CrossRef](#)]
54. Wege, H.A.; Holgado-Terriza, J.A.; Cabrerizo-Vílchez, M.A. Development of a Constant Surface Pressure Penetration Langmuir Balance Based on Axisymmetric Drop Shape Analysis. *J. Colloid Interface Sci.* **2002**, *249*, 263–273. [[CrossRef](#)] [[PubMed](#)]
55. Voinova, M.V.; Rodahl, M.; Jonson, M.; Kasemo, B. Viscoelastic Acoustic Response of Layered Polymer Films at Fluid-Solid Interfaces: Continuum Mechanics Approach. *Phys. Script* **1999**, *59*, 391–396. [[CrossRef](#)]
56. Voinova, M.V.; Jonson, M.; Kasemo, B. ‘Missing mass’ effect in biosensor’s QCM applications. *Biosens. Bioelectron.* **2002**, *17*, 835–841. [[CrossRef](#)]
57. Ivanova, N.; Starov, V.; Johnson, D.; Hilal, N.; Rubio, R. Spreading of Aqueous Solutions of Trisiloxanes and Conventional Surfactants over PTFE AF Coated Silicone Wafers. *Langmuir* **2009**, *25*, 3564–3570. [[CrossRef](#)] [[PubMed](#)]
58. Kelly-Zion, P.L.; Pursell, C.J.; Vaidya, S.; Batra, J. Evaporation of sessile drops under combined diffusion and natural convection. *Colloids Surf. A* **2011**, *381*, 31–36. [[CrossRef](#)]
59. Semenov, S.; Starov, V.M.; Rubio, R.G. Evaporation of pinned sessile microdroplets of water on a highly heat-conductive substrate: Computer simulations. *Eur. Phys. J. Spec. Top.* **2013**, *219*, 143–154. [[CrossRef](#)]
60. Zdziennicka, A.; Szymczyk, K.; Jańczuk, B.; Longwic, R.; Sander, P. Adhesion of canola and diesel oils to some parts of diesel engine in the light of surface tension components and parameters of these substrates. *Int. J. Adhes. Adhes.* **2015**, *60*, 23–30. [[CrossRef](#)]
61. Rotenberg, Y.; Boruvka, L.; Neumann, A.W. Determination of surface tension and contact angle from the shapes of axisymmetric fluid interfaces. *J. Colloid Interface Sci.* **1983**, *93*, 169–183. [[CrossRef](#)]
62. Ferreira, G.A.; Loh, W. Liquid crystalline nanoparticles formed by oppositely charged surfactant-polyelectrolyte complexes. *Curr. Opin. Colloid Interface Sci.* **2017**, *32*, 11–22. [[CrossRef](#)]
63. Guzmán, E.; Llamas, S.; Maestro, A.; Fernández-Peña, L.; Akanno, A.; Miller, R.; Ortega, F.; Rubio, R.G. Polymer–surfactant systems in bulk and at fluid interfaces. *Adv. Colloid Interface Sci.* **2016**, *233*, 38–64. [[CrossRef](#)]
64. Guzmán, E.; Fernández-Peña, L.; Ortega, F.; Rubio, R.G. Equilibrium and kinetically trapped aggregates in polyelectrolyte–oppositely charged surfactant mixtures. *Curr. Opin. Colloid Interface Sci.* **2020**, *48*, 91–108. [[CrossRef](#)]
65. Akanno, A.; Guzmán, E.; Fernández-Peña, L.; Ortega, F.; Rubio, R.G. Surfactant-Like Behavior for the Adsorption of Mixtures of a Polycation and Two Different Zwitterionic Surfactants at the Water/Vapor Interface. *Molecules* **2019**, *24*, 3442. [[CrossRef](#)] [[PubMed](#)]
66. Guzmán, E.; Fernández-Peña, L.; Luengo, G.S.; Rubio, A.M.; Rey, A.; Léonforte, F. Self-Consistent Mean Field Calculations of Polyelectrolyte-Surfactant Mixtures in Solution and upon Adsorption onto Negatively Charged Surfaces. *Polymers* **2020**, *12*, 624. [[CrossRef](#)]
67. Akanno, A.; Guzmán, E.; Ortega, F.; Rubio, R.G. Behavior of the water/vapor interface of chitosan solutions with an anionic surfactant: Effect of polymer–surfactant interactions. *Phys.-Chem. Chem. Phys.* **2020**, *22*, 23360–23373. [[CrossRef](#)]
68. Varga, I.; Campbell, R.A. General Physical Description of the Behavior of Oppositely Charged Polyelectrolyte/Surfactant Mixtures at the Air/Water Interface. *Langmuir* **2017**, *33*, 5915–5924. [[CrossRef](#)]
69. Angus-Smyth, A.; Bain, C.D.; Varga, I.; Campbell, R.A. Effects of bulk aggregation on PEI–SDS monolayers at the dynamic air–liquid interface: Depletion due to precipitation versus enrichment by a convection/spreading mechanism. *Soft Matter* **2013**, *9*, 6103–6117. [[CrossRef](#)]
70. Tummino, A.; Toscano, J.; Sebastian, F.; Noskov, B.A.; Varga, I.; Campbell, R.A. Effects of Aggregate Charge and Subphase Ionic Strength on the Properties of Spread Polyelectrolyte/Surfactant Films at the Air/Water Interface under Static and Dynamic Conditions. *Langmuir* **2018**, *34*, 2312–2323. [[CrossRef](#)]
71. Campbell, R.A.; Tummino, A.; Noskov, B.A.; Varga, I. Polyelectrolyte/surfactant films spread from neutral aggregates. *Soft Matter* **2016**, *12*, 5304–5312. [[CrossRef](#)]
72. Noskov, B.A.; Bilibin, A.Y.; Lezov, A.V.; Loglio, G.; Filippov, S.K.; Zorin, I.M.; Miller, R. Dynamic surface elasticity of polyelectrolyte solutions. *Colloids Surf. A* **2007**, *298*, 115–122. [[CrossRef](#)]

73. Aoudia, M.; Al-Haddabi, B.; Al-Harathi, Z.; Al-Rubkhi, A. Sodium Lauryl Ether Sulfate Micellization and Water Solubility Enhancement Towards Naphthalene and Pyrene: Effect of the Degree of Ethoxylation. *J. Surfact. Deterg.* **2010**, *13*, 103–111. [[CrossRef](#)]
74. Aoudia, M.; Al-Maamari, T.; Al-Salmi, F. Intramolecular and intermolecular ion–dipole interactions in sodium lauryl ether sulfates (SLES) self-aggregation and mixed micellization with Triton X-100. *Colloids Surf. A* **2009**, *335*, 55–61. [[CrossRef](#)]
75. Penfold, J.; Thomas, R.K.; Taylor, D.J.F. Polyelectrolyte/surfactant mixtures at the air–solution interface. *Curr. Opin. Colloid Interface Sci.* **2006**, *11*, 337–344. [[CrossRef](#)]
76. Langevin, D. Polyelectrolyte and surfactant mixed solutions. Behavior at surfaces and in thin films. *Adv. Colloid Interface Sci.* **2001**, *89–90*, 467–484. [[CrossRef](#)]
77. Hołysz, L.; Mirosław, M.; Terpiłowski, K.; Szcześ, A. Influence of relative humidity on the wettability of silicon wafer surfaces. *umcschem* **2008**, *63*, 223–239. [[CrossRef](#)]
78. Zdziennicka, A.; Szymczyk, K.; Krawczyk, J.; Jańczuk, B. Some remarks on the solid surface tension determination from contact angle measurements. *Appl. Surface Sci.* **2017**, *405*, 88–101. [[CrossRef](#)]
79. Bose, A. Wetting by solution. In *Wettability*; Berg, J.C., Ed.; Marcel Dekker Inc.: New York, NY, USA, 1993; pp. 149–182.
80. Staszak, K.; Wieczorek, D.; Michocka, K. Effect of sodium chloride on the surface and wetting properties of aqueous solutions of cocamidopropyl betaine. *J. Surfactants Deterg.* **2015**, *18*, 321–328. [[CrossRef](#)]
81. Gau, C.-S.; Zograf, G. Relationships between adsorption and wetting of surfactant solutions. *J. Colloid Interface Sci.* **1990**, *140*, 1–9. [[CrossRef](#)]
82. Lucassen-Reynders, E.H. Contact angle and adsorption of Solids. *J. Phys. Chem.* **1963**, *67*, 969–972. [[CrossRef](#)]
83. Kovalchuk, N.M.; Simmons, M.J.H. Surfactant-mediated wetting and spreading: Recent advances and applications. *Curr. Opin. Colloid Interface Sci.* **2021**. [[CrossRef](#)]
84. Zdziennicka, A.; Jańczuk, B. Modification of adsorption, aggregation and wetting properties of surfactants by short chain alcohols. *Adv Colloid Interface Sci* **2020**, *284*, 102249. [[CrossRef](#)]
85. Rezayi, T.; Entezari, M.H.; Moosavi, F. The variation of surface free energy of Al during superhydrophobicity processing. *Chem. Eng. J.* **2017**, *322*, 181–187. [[CrossRef](#)]
86. Zisman, W.A. Relation of the equilibrium contact angle to liquid and solid constitution. In *Contact Angle, Wettability, and Adhesion*; Fowkes, F.M., Ed.; American Chemical Society: Washington, DC, USA, 1964; pp. 1–51.
87. Extrand, C.; Kumagai, Y. An experimental study of contact angle hysteresis. *J. Colloid Interface Sci.* **1997**, *191*, 378–383. [[CrossRef](#)]
88. Bourges-Monnier, C.; Shanahan, M.E.R. Influence of evaporation on contact Angle. *Langmuir* **1995**, *11*, 2820–2829. [[CrossRef](#)]
89. Hu, H.; Larson, R.G. Analysis of the microfluid flow in an evaporating sessile droplet. *Langmuir* **2005**, *21*, 3963–3971. [[CrossRef](#)]
90. Senses, E.; Black, M.; Cunningham, T.; Sukhishvili, S.A.; Akcora, P. Spatial ordering of colloids in a drying aqueous polymer droplet. *Langmuir* **2013**, *29*, 2588–2594. [[CrossRef](#)]
91. Soulié, V.; Karpitschka, S.; Lequien, F.; Prené, P.; Zemb, T.; Moehwald, H.; Riegler, H. The evaporation behavior of sessile droplets from aqueous saline solutions. *Phys. Chem. Chem. Phys.* **2015**, *17*, 22296–22303. [[CrossRef](#)] [[PubMed](#)]
92. Trybala, A.; Okoye, A.; Semenov, S.; Agogo, H.; Rubio, R.G.; Ortega, F.; Starov, V.M. Evaporation kinetics of sessile droplets of aqueous suspensions of inorganic nanoparticles. *J. Colloid Interface Sci.* **2013**, *403*, 49–57. [[CrossRef](#)]
93. Deegan, R.D.; Bakajin, O.; Dupont, T.F.; Huber, G.; Nagel, S.R.; Witten, T.A. Contact line deposits in an evaporating drop. *Phys. Rev. E* **2000**, *62*, 756–762. [[CrossRef](#)]
94. Moroi, Y.; Rusdi, M.; Kubo, I. Difference in surface properties between insoluble monolayer and adsorbed film from kinetics of water evaporation and BAM image. *J. Phys. Chem B* **2004**, *108*, 6351–6358. [[CrossRef](#)]
95. Lunkenheimer, K.; Zembala, M. Attempts to Study a Water Evaporation Retardation by Soluble Surfactants. *J. Colloids Interface Sci.* **1997**, *188*, 363–371. [[CrossRef](#)]
96. Nguyen, T.A.H.; Biggs, S.R.; Nguyen, A.V. Manipulating colloidal residue deposit from drying droplets: Air/liquid interface capture competes with coffee-ring effect. *Chem. Eng. Sci.* **2017**, *167*, 78–87. [[CrossRef](#)]
97. Doganci, M.D.; Sesli, B.U.; Erbil, H.Y. Diffusion-controlled evaporation of sodium dodecyl sulfate solution drops placed on a hydrophobic substrate. *J. Colloid Interface Sci.* **2011**, *362*, 524–531. [[CrossRef](#)] [[PubMed](#)]
98. Girard, F.; Antoni, M.; Faure, S.; Steinchen, A. Evaporation and marangoni driven convection in small heated water droplets. *Langmuir* **2006**, *22*, 11085–11091. [[CrossRef](#)]
99. Girard, F.; Antoni, M.; Sefiane, K. On the effect of Marangoni flow on evaporation rates of heated water drops. *Langmuir* **2008**, *24*, 9207–9210. [[CrossRef](#)] [[PubMed](#)]
100. Picknett, R.G.; Bexon, R. The evaporation of sessile or pendant drops in still air. *J. Colloid Interface Sci.* **1977**, *61*, 336–350. [[CrossRef](#)]